

---

GUIDANCE FOR STRATOSPHERIC  
TEMPERATURE PRODUCTS:  
COMPARING COSMIC RADIO OCCULTATION AND AIRS  
HYPER SPECTRAL INFRARED SOUNDER DATA

---

BY

MICHELLE L. FELTZ

A THESIS SUBMITTED IN PARTIAL FULFILLMENT OF

THE REQUIREMENTS FOR THE DEGREE OF

MASTER OF SCIENCE

(ATMOSPHERIC AND OCEANIC SCIENCES)

AT THE

UNIVERSITY OF WISCONSIN-MADISON

2015

## ADVISOR APPROVAL PAGE

ADVISOR TITLE:

STEVE ACKERMAN  
PROFESSOR, UNIVERSITY OF WISCONSIN-MADISON DEPARTMENT OF ATMOSPHERIC AND  
OCEANIC SCIENCES  
DIRECTOR, COOPERATIVE INSTITUTE FOR METEOROLOGICAL SATELLITE STUDIES

---

ADVISOR SIGNATURE

---

DATE

## DEDICATION

To the One who formed Earth, who knows the complex workings of life, and  
who set forces in place that govern the smallest subatomic particles all the way to the  
expansive heavens,

and to an unnamed best friend  
who listened to my many ramblings on not only subjects motivated by this work,  
but also those motivated by life's happenings during my Master's work.

## TABLE OF CONTENTS

<b>1. INTRODUCTION: STRATOSPHERIC TEMPERATURES</b>	<b>1</b>
A. IMPORTANCE	1
B. CURRENT MEASUREMENT STATUS	1
C. AVAILABLE DATASETS	2
<b>2. SCIENCE QUESTIONS AND OBJECTIVES</b>	<b>5</b>
<b>3. BACKGROUND</b>	<b>7</b>
A. RADIO OCCULTATION	7
B. HYPERSPECTRAL INFRARED SOUNDERS	9
<b>4. DATA</b>	<b>11</b>
A. UCAR COSMIC	11
B. NASA AIRS	11
C. CRIMSS	12
D. CARBON TRACKER	12
E. ERA-INTERIM	13
<b>5. STRATOSPHERIC TEMPERATURES FROM COSMIC AND AIRS</b>	<b>14</b>
A. METHODS	14
i. Zonally Averaged Temperature Statistics	14
B. COSMIC AND AIRS DESCRIPTIVE STATISTICS	14
B. MEAN AIRS – MEAN COSMIC RESULTS	18
<b>6. INVESTIGATION OF COSMIC AND AIRS DIFFERENCES: TOWARDS A QUANTIFICATION OF RO AND IR SOUNDER ACCURACY</b>	<b>20</b>
A. METHODS	20
i. RO and IR Sounder Matchup Methodology	20
ii. RTM Methodology and Perturbation Study Setup	21
iii. Averaging Kernel Calculation and Application	23
iv. Statistics	24
B. CASE STUDY MATCHUPS	25
C. RADIATIVE TRANSFER MODEL PERTURBATION STUDY	26
D. REVISITING MEAN AIRS – MEAN COSMIC: ELIMINATION OF SAMPLING DIFFERENCES	29
E. ADDRESSING DIFFERENCES IN VERTICAL RESOLUTION	31
F. COMPARISONS IN RADIANCE AND TEMPERATURE SPACE	32
<b>7. DISCUSSION</b>	<b>36</b>
<b>8. CONCLUSIONS</b>	<b>39</b>
<b>APPENDIX A: ACRONYMS</b>	<b>41</b>
<b>REFERENCES</b>	<b>42</b>
<b>TABLES</b>	<b>46</b>
<b>FIGURES</b>	<b>49</b>

## 1. INTRODUCTION: STRATOSPHERIC TEMPERATURES

### A. IMPORTANCE

Upper-air temperature is defined by The World Meteorological Organization as an essential climate variable (GCOS, 2011). A recent Global Climate Observing System report (2011) quotes,

“Upper-air temperatures are crucial for distinguishing the various possible causes of climate change and for the validation of climate models, and they can potentially be used for improved understanding of long-term variability in atmospheric circulation. Changes in upper-air temperatures are also crucial for understanding changes in water vapour in the lower stratosphere and for reconciling ozone trends between different satellite instruments.”

These statements highlight the important utility of an accurate, climate-quality stratospheric temperature dataset.

### B. CURRENT MEASUREMENT STATUS

A recent Nature paper by Thompson et al. (2012), titled “The Mystery of Recent Stratospheric Temperature Trends”, brings to light the differences among current climate model output and available stratospheric temperature datasets derived from satellite observations. Though the Intergovernmental Panel on Climate Change (IPCC) Working Group I Fifth Assessment Report (AR5) states it is *virtually certain* that since the mid-20<sup>th</sup> century a cooling of the stratosphere has occurred globally, the report goes on to note “substantial disagreement exists among available estimates as to the rate of temperature changes” and that low confidence is placed in the rate of change and its vertical structure around the globe. Since the AR4, uncertainties of current satellite and radiosonde datasets have been brought to a higher level of attention. More recent work that compares temperature analyses from the ERA-40, MERRA, JRA-55, and ERA-Interim concludes

that the middle stratosphere is the atmospheric region containing the largest uncertainties in temperature (Simmons et al., 2014).

### **C. AVAILABLE DATASETS**

The longest stratospheric temperature datasets are provided by radiosondes, Stratospheric Sounding Units (SSUs), and Microwave Sounding Units (MSUs). As MSUs only provide one channel that peaks within the lower stratosphere, the latest IPCC AR5 did not consider this as a source for stratospheric temperature records. The Stratospheric Sounding Unit took measurements from 1979 to 2006 while radiosonde networks have been taking measurements since ~1970 up to the current day; however, these records each have limitations in their applications, especially for long-term trends and climate analyses (Seidel et al., 2011).

Radiosondes were originally intended for use in numerical weather forecasting, created with a goal of obtaining real-time tropospheric measurements, rather than stable stratospheric measurements suitable for climate studies. Radiosondes have limited temporal and spatial coverage over the globe with a bias towards Northern Hemisphere land in comparison to satellite measurements (Sun et al., 2013). Though the sparser temporal sampling characteristic of this dataset would not necessarily limit a climate analysis, the lack of a uniform global representation of data is a large disadvantage. Radiosondes often fail to reach above 50 hPa (Seidel et al., 2011), and studies have demonstrated that inconsistencies in measurements from different radiosonde types are larger at stratospheric levels than at lower levels of the atmosphere (Gaffen, 1994). Radiosonde differences such as these have been highlighted and assessed in various studies (He et al., 2009; Sun et al., 2010, 2013; Philipona et al., 2013). In addition,

general warming and cooling temperature biases have been cautioned to exist in radiosonde datasets (Haimberger et al., 2008).

SSUs, which currently offer the only long-term near-global temperature dataset above the lower stratosphere, have provided measurements that are difficult and disadvantageous to use in climate studies. The SSU instruments used a pressure modulator radiometer technique, and therefore their data record requires very careful calibration due to issues such as instrument differences, leaky carbon dioxide (CO<sub>2</sub>) cells, increasing atmospheric CO<sub>2</sub> amounts, and changing equatorial crossing times of the satellite platforms. This makes the SSU datasets subject to large uncertainties (Randel et al., 2009; Seidel et al., 2011). While these issues are great obstacles when attempting to create a continuous temperature record from the SSU series, multiple studies have made efforts to overcome these obstacles and minimize errors in the dataset (Shine et al., 2008; Randel et al., 2009; Wang et al., 2012). However, even with minimized errors, larger uncertainties associated with the SSU temperature records persist.

A more recently established, operational data source for stratospheric temperatures has been hyperspectral infrared (IR) and microwave (MW) sounders. Hyperspectral infrared sounders, such as AIRS, IASI, and CrIS, use onboard calibration techniques and therefore are able to make brightness temperature measurements with greatly reduced uncertainties in comparison to other sounders (Aumann et al., 2003; Tobin et al., 2013). These instruments have many channels whose weighting functions peak at levels spanning the troposphere into the stratosphere and thus provide information on the vertical structure of the atmosphere. While hyperspectral IR sounder measurements have a high accuracy, the derived temperature retrievals often have larger

uncertainties due to the ill-posed nature of the retrieval problem (Rodgers, 1976).

Additionally, past underlying purposes for retrieving temperatures have been for real-time operational forecasting, where speed of the retrieval scheme is a valued factor and a focus is set on accuracy within the troposphere, rather than the middle atmosphere. The retrieval of climate quality stratospheric temperatures has not been formalized in the literature, though studies have shown demonstrations (Hoffmann and Alexander, 2009).

Another relatively new form of technology that has been providing temperature profile products is radio occultation (RO). Based off of GPS signal phase delays between GPS transmitters and low earth orbiting receivers, measurements from RO are traceable to the International System of Units (SI) standard of time and thus have been proposed as a candidate for long-term climate records (Mannucci et al., 2006; Leroy et al., 2006). High stability of the observations is provided by the accuracy and reliability of the RO instrument clocks used to monitor the radio occultations (Leroy et al., 2006; Foelsche et al., 2008, 2011b; Steiner et al., 2011). While RO observations from different instruments and networks do not have inter-calibration issues and should have similar observational accuracies due to their common time basis, the various processing schemes offered by different data centers introduce structural uncertainties associated with derived RO products (Ho et al., 2009, 2012; Steiner et al., 2013). Though RO data is acclaimed to be most reliable in the upper troposphere, lower stratosphere (UTLS) region, current RO temperature products may not offer the accuracy needed for climate studies of the temperatures throughout the stratosphere. Work done by Wee and Kuo (2014) exemplifies the current underutilization of RO data for stratospheric studies.

## 2. SCIENCE QUESTIONS AND OBJECTIVES

A question motivated by the above discussion is, ‘Are hyperspectral IR sounders and radio occultation suitable for stratospheric temperature climate studies?’, or split into two questions:

- a) Are IR sounder and RO sampling characteristics adequate for climate studies?
- b) Are current temperature profile products from IR sounders and RO accurate enough for climate studies?

To address these questions, RO data from the COSMIC mission and hyperspectral infrared sounder data from the Atmospheric Infrared Sounder (AIRS) are analyzed. In the first section, the complete COSMIC and AIRS derived temperature datasets over a 6-year time period are studied. Six years is chosen because of its complete overlap between the AIRS program, COSMIC mission, and other datasets necessary for subsequent forward calculations, i.e. the calculation of radiances from temperature. Descriptive statistics such as means and intra-monthly standard deviations as well as differences of the mean temperatures are computed on monthly and 5-degree zonal scales. Though simplistic, these results are essential in understanding the characteristics of the datasets, which differ in many aspects due to the different measurement techniques and satellite orbits of IR sounders and RO.

In the second section AIRS and COSMIC temperature profile product agreement is quantified on various time and space scales, and the sources of their differences are investigated. This is facilitated by the use of a profile-to-profile matchup methodology as well as forward calculations of the matchup temperature dataset. While IR sounder and RO products are in theory traceable to SI standards, no such formalism has yet been

established in the literature, though it is the NASA CLARREO mission to do so for future climate observations. Additionally, though model fields and radiosondes can be attractive options for temperature references, models are often not independent data sources, and radiosondes lack sufficient spatial coverage and contain systematic measurement errors at higher altitudes (Seidel et al., 2011). Thus, in this study AIRS and COSMIC temperature products are compared against each other. Using the matchup temperatures as input to the forward model, COSMIC and AIRS calculated radiances are compared to AIRS measured radiances which are used here as a validation reference. In this way, the low IR radiance measurement uncertainty is taken advantage of and a method for establishing SI traceability between IR measurements and RO temperature products is demonstrated through the forward calculation process.

### 3. BACKGROUND

#### A. RADIO OCCULTATION

Radio occultation is an active, remote-sensing, limb sounding technology that uses electromagnetic pulses that are sent out by the GPS constellation of satellites and detected by receivers on low earth orbiting satellites (Kursinski et al., 1997). As the electromagnetic pulses propagate through the earth's atmosphere, they are refracted according to Snell's Law. This wave refraction, a Doppler shift, and the travel time of the signal to the receiver combine to create a total phase delay which can be transformed into a bending angle as a function of impact parameter using knowledge of the satellite orbit geometry (Kursinski et al., 1997). Using an Abel transform, refractivity as a function of altitude is then calculated using approximations relating to Earth's non-spherical shape, horizontal density gradients, and the ionosphere's free electron content (Kursinski et al., 1997). Approximations such as these have been shown to cause errors in profiles with increasing obliquity, or less verticality (Foelsche et al., 2011a). To a first order estimate for microwave wavelengths, the atmospheric refractivity,  $N$ , is given by

$$N = 77.6 \left( \frac{P}{T} \right) + 3.73 \times 10^5 \left( \frac{P_w}{T^2} \right) + 4.03 \times 10^7 \left( \frac{n_e}{f^2} \right) + 1.4W ,$$

where  $P$  is pressure and  $P_w$  is water vapor partial pressure,  $T$  is temperature,  $n_e$  is electron number,  $f$  the transmitter frequency, and  $W$  the condensed water mass (Kursinski et al., 1997). The fourth term, describing scattering by liquid water, is very small and generally negligible, and if a dry temperature retrieval is being performed, then the second, moist atmospheric term is neglected. The first order ionospheric effect given in the third term has been introduced in the literature as an increasing concern for temperature retrieval accuracy and is corrected for by using the knowledge that the

ionosphere's dispersive nature affects the two GPS signals in different amounts (Syndergaard, 2000; Mannucci et al., 2011; Danzer et al., 2013). While the ionospheric contribution is removed from the measurements at higher altitudes by combing the two frequencies prior to the temperature derivation, amplified noise errors from the processing propagate downwards in altitude and can thus affect the temperature retrieval at lower levels (Wee and Kuo, 2014). Density can be obtained by proportionality to the first, dry atmospheric contribution term. Pressure is then calculated using the hydrostatic equation and transformed into temperature using the ideal gas law. Temperature profiles calculated with the assumption of zero atmospheric water vapor are called 'dry temperature' and accumulate error in the troposphere where the presence of water vapor is non-negligible.

Radio occultation can offer discrete profile measurements with a global distribution depending on the satellite orbit geometry and is not biased to have more frequent observations over land, unlike the WMO radiosonde network. RO also gives observations for given geographic locations that are not biased to occur for only certain times of the day, such as sounders that operate from satellites with sun-synchronous orbits at fixed local times or WMO radiosondes launched only at 00 and 12 UTC. Depending on the altitude, derived temperature profiles have a vertical resolution from 0.5–2 km and a horizontal resolution from 160–320 km (Kursinski et al., 1997). Single profile observational RMS errors are estimated to be 0.7 – 1K between 8 – 25km, while for climatologies the observational, sampling, and systematic errors sum up to be within 0.15K in this altitude range in the low to mid latitudes (Steiner et al., 2011). Initialization

and ionospheric residual errors are the main contributors to systematic errors above ~25km (Steiner et al., 2011).

### B. HYPERSPECTRAL INFRARED SOUNDERS

Hyperspectral infrared sounders are passive, remote sensing instruments that measure radiation at infrared wavelengths emitted by Earth using spectrometers such as Fourier transform spectrometers (e.g. Michelson interferometer) or diffraction gratings with optics. By utilizing rotating scene mirrors, these instruments are able to scan Earth in wide swaths and self-calibrate with spectral and radiometric standards such as onboard blackbodies and views to deep space (Aumann, 2003). From observed infrared radiances, a non-scattering radiative transfer equation can be used to retrieve temperature profiles. The upwelling, monochromatic radiance from a clear, non-scattering atmosphere is given by the following equation:

$$R_v = \epsilon_v B_v(T_s) \tau_v(p_s \rightarrow 0, \theta_{sat}) + \int_{p_s}^0 B_v(T(p)) \frac{d\tau_v(p \rightarrow 0, \theta_{sat})}{dp} dp + \dots$$

$$F_v^d \rho_v^t \tau_v(p_s \rightarrow 0, \theta_{sat}) + \frac{H_v}{\sec(\theta_{sun})} \tau_v(0 \rightarrow p_s, \theta_{sun}) \rho_v^s \tau_v(p_s \rightarrow 0, \theta_{sat}),$$

where  $\epsilon_v$  is the surface emissivity,  $B_v(T_s)$  the Planck function,  $\tau_v$  the transmittance,  $\theta_{sat}$  the satellite zenith angle,  $F_v^d$  the down-welling thermal flux,  $\rho_v^t$  the surface reflectance,  $H_v$  the solar irradiance incident at the top of the atmosphere, and  $\rho_v^s$  the surface solar reflectance. From left to right respectively, the terms on the right side of the equation represent the surface blackbody emission, atmospheric emission, down-welling atmospheric emission reflected by the surface, and reflected solar irradiance (Strow, et al., 2003). Due to the IR spectrum's sensitivity to the presence of clouds, brightness temperature (BT) measurements from hyperspectral IR sounders are commonly

combined with MW brightness temperatures to retrieve vertical temperature profiles (Susskind et al., 2011; Liu et al., 2012). For IR BTs measured in cloudy scenes, a microwave-only retrieval may be used as a first-guess estimate.

Housed on polar orbiting satellites, infrared sounders take measurements in large swaths that cover the globe approximately twice daily. A temperature profile from AIRS has a horizontal resolution of  $\sim 50$  km while there are 101 fixed pressure levels that span the entire atmosphere up to 0.005hPa (Susskind et al., 2003). Specification requirements for IR sounder temperature profiles are typically defined for 3 to 5 km slabs depending on the pressure level and have required accuracies of  $\sim 1.5$ K from 300hPa – 1hPa and  $\sim 3.5$ K from 1hPa – 0.5hPa (Nalli et al., 2014; Divakarla et al. 2014).

## **4. DATA**

### **A. UCAR COSMIC**

The US/Taiwanese COSMIC, or Taiwan's Formosa Satellite Mission #3 (FORMOSAT-3), network is a mission consisting of six radio receivers on low earth orbiting satellites in circular 72-degree inclination orbits that has been ongoing since April 2006 (Anthes et al., 2008). The COSMIC network produces around 1000–2000 profiles per day with a relatively sparser sampling of the tropics than other latitudes. Due to lost contact to various satellites and the FM3 satellite permanently since August 2010, the daily number of profiles has decreased over time. Data is obtained from the UCAR COSMIC Data Analysis and Archive Center (CDAAC). The post-processed dry temperature product from the 'cosmic' mission version 2010.2640, labeled "atmPrf", is used in this study. An updated version of the COSMIC data, 'cosmic2013', has become available that includes many corrections, including one for a hemispheric bias that was detected between COSMIC and GNSS Receiver for Atmospheric Sounding (GRAS) data (Feltz, 2014b). ERA-Interim reanalysis model data that are collocated with the COSMIC mission profiles, labeled "eraPrf", are also used from the CDAAC. Applied quality control consists of excluding profiles marked 'bad'.

### **B. NASA AIRS**

NASA's AIRS/AMSU sensors are located on the Earth Observing System Aqua satellite and have been collecting data since September 2002. Derived temperatures and measured radiances are obtained from the Goddard Earth Sciences Data and Information Services Center. The Level-2 (L2), version 6.0 Support Product (AIRX2SUP.006) temperature granules as well as the Level-3, version 6.0, daily 1x1 degree gridded

temperature products (AIRX3SPD.006) are used. Quality control of the L2 retrievals consists of using the quality flag labeled “Pbest”, which determines how deep into the atmosphere the satellite retrieval is considered to be valid (Susskind et al., 2011). The AIRS L1B measured radiance files used are AIRIBRAD version 5.

### **c. CRIMSS**

Cross-Track Infrared and Microwave Sounder Suite (CrIMSS) data from the Suomi NPP satellite are available from April 2011 to the current day and are obtained from NOAA CLASS. The 42 temperature layer Atmospheric Vertical Temperature Profile product is used (JPSS Configuration Management Office, 2012). CrIMSS data used in this study are version Mx5.3 and are from the time when the product was still in provisional status prior to major subsequent upgrades (Divakarla et al., 2014). Quality control is applied using the overall retrieval quality flag—non-converged retrievals are not included in the analysis.

### **d. CARBON TRACKER**

Carbon dioxide (CO<sub>2</sub>) data is obtained from CarbonTracker (CT), NOAA’s Earth System Research Laboratory (ESRL) CO<sub>2</sub> measurement and modeling system. CarbonTracker data is collected from the ESRL greenhouse gas observational network and collaborating institutions. Used in this study is version CT2013 which is available for 2000-2012 as global 3x2 degree gridded monthly CO<sub>2</sub> Mole Fractions, which are made by using optimized surface fluxes and simulated atmospheric transport (<http://carbontracker.noaa.gov>). More information on CarbonTracker, as well as an evaluation of its model output using aircraft observations, can be found in Peters et al. (2007).

### **E. ERA-INTERIM**

Ozone, skin temperature, and surface pressure are obtained from ECMWF's ERA-Interim reanalysis (<http://www.ecmwf.int/en/research/climate-reanalysis/era-interim>). The model is available at 6 hourly increments at ~80 km resolution. The 0.75-degree gridded model level product is used in preference to the pressure level product, as the model levels report up to higher altitudes than the pressure levels. The ERA-Interim is further described in Dee et al. (2011) and details of its output in Berrisford et al. (2011).

## 5. STRATOSPHERIC TEMPERATURES FROM COSMIC AND AIRS

### A. METHODS

#### I. ZONALLY AVERAGED TEMPERATURE STATISTICS

AIRS and COSMIC data are averaged over 2007-2012 on monthly and 5-degree zonal scales. AIRS Level 3, daily 1x1 degree gridded ascending and descending orbit products are averaged together to obtain the mean temperatures. The standard deviation of the AIRS retrievals used to make the gridded mean products is estimated by assuming that each 1x1 degree daily profile is independent. COSMIC data, available as individual profiles, are first interpolated to the AIRS 101 levels and then similarly averaged into monthly 5-degree latitude zones. Because COSMIC profiles were found to have a uniform distribution through time and longitude, smaller binning was not applied prior to the 5-degree latitude averaging.

Uncertainties of the mean temperatures are calculated as the standard deviation divided by the square root of the number of samples. Seasonal climatologies of the averaged temperatures are calculated by taking a mean through each season over the 6-year time period 2007 - 2012.

### B. COSMIC AND AIRS DESCRIPTIVE STATISTICS

Figure (Fig) 1 shows example daily sampling patterns of AIRS and COSMIC for 1 January 2007. In Fig 1's top panel, COSMIC profile tangent point locations illustrate the pseudo-random point sampling of RO. Fig 1's bottom panel shows ascending and descending AIRS counts and illustrates the broad horizontal IR sounder swath coverage. While IR sounders may have an advantage over RO for horizontal coverage on shorter time scales, when considering temperature on monthly and zonally averaged scales, the sampling of RO and IR both seem to be adequate. COSMIC and AIRS number of

samples at 1hPa are shown in Fig 2's top and bottom panel respectively. This pressure level's number of samples is representative for levels down through the lower stratosphere. Generally, the number of AIRS samples is three orders of magnitude larger than the COSMIC number of samples with the exception being over the poles and an atypical time period around January 2010. COSMIC sample numbers have local maxima around  $\pm 50$  and  $\pm 20$  degrees latitude. Due to lost contact to various satellites in the COSMIC constellation, including a permanent loss to satellite FM3 since August 2010, there are larger variations in the temporal distribution as well. While different RO missions have different sample numbers and patterns, a constellation such as COSMIC, or the planned follow-on mission, COSMIC-2, offers adequate sampling on the time and space scales shown.

Figure 3 shows the standard deviations at 1hPa and 35hPa, corresponding to the stratopause and middle stratosphere respectively. AIRS and COSMIC show similarity in that maxima are seen in polar wintertime, which dynamically makes sense due to the facts that 1) a westerly stratospheric jet is developed over the winter pole and 2) the vertical propagation of Rossby wave disturbances (which would broaden the distribution of experienced temperatures) only happens into areas of westerly mean winds. Differences seen in the standard deviations, for example how COSMIC's is lower at almost all latitudes on both levels, could aid in diagnosing the sources of AIRS and COSMIC differences at these levels.

Mean temperatures and their differences are shown in Fig 4. The pattern of mean temperatures shown is in part a product of the Brewer Dobson Circulation, the dominating stratospheric circulation that can crudely be described as a pole to equator

circulation where air rises in the tropics and descends in the polar regions. This pattern of stratospheric temperatures on such monthly, zonal scales is discussed in depth in analyses such as Young et al. (2010) and more originally Yulaeva et al. (1994) by using the MSU and SSU sounder data. AIRS and COSMIC are both able to capture the dominant features of this seasonally varying circulation. Interesting features seen on such scales are signatures of sudden stratospheric warmings at the northern pole, more prominently at 1hPa. Such phenomena are recorded to have occurred in the winters of 2009, 2010, and 2011, with a minor one occurring in 2008. While AIRS seems to better detect such phenomena on monthly, 5-degree zonally averaged scales, hints of warming episodes are still seen by COSMIC. Fig 4 bottom panels show the mean AIRS minus mean COSMIC difference. At 1hPa in the high latitude spring to summer time frame AIRS is colder than COSMIC by up to 20K, while in the tropics AIRS is often warmer than COSMIC by over 4K at some points. At 35hPa, AIRS and COSMIC generally agree within 2K with the exception of Antarctic winter time periods, where AIRS is again colder than COSMIC.

Fig 5 again depicts AIRS and COSMIC number of samples, but for a specific Antarctic latitude zone and shows that AIRS and COSMIC both give adequate coverage throughout the height of the stratosphere. The height where sample numbers go to zero in the upper atmosphere for COSMIC varies with the season close to the poles—the northern and southern hemisphere (NH and SH) patterns being out of phase. In the Antarctic, sampling coverage reaches highest in the atmosphere during October, November, and December.

Similar plots of standard deviations are shown in Fig 6. COSMIC records different standard deviations in the lower troposphere in part due to water vapor

contamination of the dry temperature product – seen most notably in the tropics.

COSMIC also records much higher standard deviations above 1hPa in the mesosphere.

Figures 7 and 8 show corresponding mean temperatures and a difference of the AIRS and COSMIC means for 5 latitude zones. A roughly mirrored but temporally offset structure is seen across the equator in mean temperatures as well their differences; however, distinctions between hemispheres are seen. The larger, near surface differences between COSMIC and AIRS that are due to the RO dry temperature water vapor cold bias vary in magnitude and vertical extent with latitude, being most notable in the tropics. In the tropical and mid-latitude stratosphere differences are smaller, generally below 5K with the exception of the upper stratosphere above ~5hPa, where differences occur more regularly for certain seasons and zones, e.g. SH spring to summertime months seen in Fig 8. Vertical layering of the difference values seen throughout the tropical zone and near tropical mid-latitudes might help diagnose issues that either instrument has with resolving the stratopause or tropopause. For example, the tropical stratopause region is associated with AIRS typically being warmer than COSMIC. In Fig 7 the polar zones reveal much larger differences at more temporal periodic intervals, as well as very large magnitude differences above 20K in the upper stratosphere, lower mesosphere during NH wintertime months. In the SH polar zone the wintertime AIRS vertical oscillation (discussed in Feltz et al., 2014b) can be seen in the mean temperature as well as the difference extending throughout most of the atmosphere—most clearly in the middle and upper stratosphere.

Lastly, Fig 9 shows the 6-year period seasonal temperature climatology over pressure and latitude for December, January, and February (DJF) and for June, July, and

August (JJA). The latitudinal extent of the SH wintertime AIRS vertical oscillation is seen to cover about  $-50^{\circ}\text{N}$  to  $-90^{\circ}\text{N}$ . A feature of the AIRS-COSMIC difference common to both seasons is the pair of positive regions located around  $\pm 30^{\circ}\text{N}$  above the 1 hPa pressure level. In wintertime hemispheres just under the 1hPa level AIRS is seen to be colder than COSMIC by up to and over 10K, as seen in previous mean temperature figures.

The above figures illustrate that on 5-degree zonal and monthly time scales characteristic differences between AIRS and COSMIC can be identified. While similarities do exist between AIRS and COSMIC data in their ability to capture atmospheric temperature variations across latitude and time, the magnitude of the differences within stratospheric regions warn that either one or both of the AIRS and COSMIC temperature datasets contain large errors that inhibit the dataset from being useful in climatic studies within various stratospheric regions.

#### **B. MEAN AIRS – MEAN COSMIC RESULTS**

Fig 10 shows histograms of the mean AIRS minus mean COSMIC differences overlaid with normal distributions for the  $\sim 1\text{hPa}$  and  $\sim 35\text{hPa}$  pressure level for global and tropical regions (see Figure 4 for corresponding maps). Global differences at 1hPa are clearly non-Gaussian and are largely skewed to negative temperature differences. The more Gaussian shaped global 35hPa histogram suggests that random processes could dominate error sources, but the map seen in Fig 4 suggests that multiple, different, non-random processes could be contributing to the differences sources—the differences have a visibly characteristic spatiotemporal pattern. The tropical,  $\pm 30^{\circ}\text{N}$  region's histograms seen in Fig 10's lower panels are somewhat more normally distributed, skewed slightly to

more positive temperature differences at 35hPa with AIRS being warmer than COSMIC. None of the distributions as determined by a chi-squared goodness of fit test are significantly normal. The mean, standard deviation, and uncertainty of the mean are shown in figure titles. The number of samples,  $N$ , is defined as the number of monthly, zonally averaged mean temperatures within the defined latitude range for which the histogram is made. For both pressure levels, the uncertainty of the mean is lower for the tropical region. The histogram of the subset tropical temperature differences demonstrates the idea that different regions can be associated with varying uncertainties in datasets and can offer different opportunities for trending studies.

Multiple hypotheses could explain the large AIRS-COSMIC differences in the winter polar zones seen at both pressure levels (seen in Fig 4). Possible contributors to these differences could include the sparse polar sampling coverage by AIRS or COSMIC, a negative refractivity screening in the COSMIC temperature processing that could produce a warm temperature bias (Foelsche, 2014), and the AIRS version 6 ‘vertical oscillation’ that was identified in the Antarctic winter months (Feltz et al., 2014b). More generally, such a difference between means could possibly be due to 1) sampling differences of the RO and IR sounder in time and space, 2) measurement errors, and 3) differences due to temperature retrieval errors. Section 6 investigates the possibilities of these error sources.

## 6. INVESTIGATION OF COSMIC AND AIRS DIFFERENCES: TOWARDS A QUANTIFICATION OF RO AND IR SOUNDER ACCURACY

### A. METHODS

#### I. RO AND IR SOUNDER MATCHUP METHODOLOGY

The RO and IR temperature profile-to-profile matchup methodology is described in detail in Feltz et al. (2014a). A raypath profile technique accounts for the RO horizontal resolution and unique profile geometry in order to minimize spatial mismatch error, while a one-hour time restriction between profile occurrences minimizes temporal mismatch error. The matchup location is defined by the latitude and longitude of the RO profile pressure level that's closest to 100hPa. Fig 11 shows an example daily distribution of matchups. The number of matchups for a given day is a function of the IR and RO satellite orbits and varies with season and latitude. The polar-orbiting nature of the satellites housing the IR instruments in addition to the fact that COSMIC has fewer profile events in the tropics, cause the matchups to be densest in the polar regions. For COSMIC and AIRS, there are ~300 global matchups per day and ~7,000-11,000 per month.

In this study, the AIRS measured radiances are added as a new element of the matchup dataset. A profile of AIRS radiances for all channels is extracted due to the height dependence of the closest AIRS fields of regard to the RO matchup profile. Specifically, the AIRS L1B 3x3 radiance 'golfball' (which corresponds to a L2 retrieval field of view) that is closest to the matchup profile is saved. An example figure of such a radiance profile is seen in Fig 12. Then, when selecting the matchup radiances for a specific AIRS channel, the 3x3 golfball mean that is closest in height to the channel's

weighting function maximum is selected. Using this method, radiances for different channels are represented by measurements taken at different latitudes and longitudes (based on the RO profile geometry).

Quality control of the matchup cases (beyond the quality flags marking good or bad AIRS and COSMIC data) consists of excluding AIRS or COSMIC temperature profiles without complete information on the AIRS 101 levels between 1 and 100hPa.

## II. RTM METHODOLOGY AND PERTURBATION STUDY SETUP

Forward calculations of AIRS radiances using the matchup dataset are performed using the radiative transfer model (RTM) Optimal Spectral Sampling (OSS) (Moncet et al., 2008). To investigate the sensitivity of the calculated radiances to various aspects of the forward calculation methodology, two categories of perturbations are performed—one on temperature and one on carbon dioxide due to the focus of this study around the 15-micron carbon dioxide band. For both studies, the control case is defined using the 1986 version Air Force Geophysics Laboratory (AFGL) mid-latitude winter temperature, the mean 44-46°N January 2007 carbon dioxide, and the mean NH mid-latitude January 2007 ozone, water vapor, and skin temperature as determined from the matchup set forward calculation input described below.

For each matchup case, radiances for both AIRS and COSMIC temperatures are calculated using all other similar model parameters. Table 1 shows OSS model input parameters and describes from what source they are defined. The pressure profile and top-of-atmosphere (toa) pressure, defined using the AIRS 101 pressure levels, as well as the solar zenith angle, are constant for every matchup case. Surface pressures, skin temperatures, and ozone profiles are defined using ERA-Interim 6-hourly values that are

spatiotemporally closest to the matchup locations. Because the ERA-Interim ozone product is reported on model levels, a conversion of the ozone profile model levels to pressure levels is performed using a defined technique from ECMWF (Berrisford et al., 2011). Water vapor profiles are defined by the ERA-Interim as well; however, they are not obtained from ECMWF but from UCAR and are interpolated by CDAAC processing to the location of the COSMIC profile. Because the ERA-Interim products are only reported up to ~1 km and do not cover the entire vertical range needed for OSS input, the AFGL Atmospheric Constituent Profiles of ozone and water vapor are used as ‘climatology’ that’s added at altitudes above and below the ERA-Interim profiles. The day of year and latitude of the matchup determines which AFGL model atmosphere is used, i.e. subarctic winter/summer, mid-latitude winter/summer, or tropical.

CarbonTracker monthly, 2-degree zonal averages are used to define the carbon dioxide profiles, and for the vertical levels above and below the profile where there is no available information, the profile is extended to be constant with height. The slant angles, or view angles, that the COSMIC and AIRS radiances are calculated for are taken from the AIRS measured radiance files that correspond to the matchup AIRS temperature profiles. Specifically, the mean scan angle of the AIRS L1B 3x3 radiance ‘golfball’ for which the AIRS matchup temperature profile is retrieved is used.

Lastly, the COSMIC and AIRS temperature profiles for which the forward calculations are performed need to be merged with AFGL model temperatures. Depending on the matchup case and latitude zone, there can be ‘discontinuities’, or large, above 10K jumps in the COSMIC or AIRS input temperature profile between pressure levels where the information comes from two different sources (i.e. the climatology and

either COSMIC or AIRS temperatures). This ‘discontinuity phenomenon’ is more common in the COSMIC input temperature (since COSMIC does not report values at as high of altitudes as AIRS) for NH mid-latitude winter cases. The effect of this discontinuity phenomenon on the radiance calculations is investigated using a perturbation study in Section 6c. In order that this phenomenon might have less of an effect on the comparison of COSMIC and AIRS calculated radiances, climatology is added to the AIRS profile wherever it is added to COSMIC.

### III. AVERAGING KERNEL CALCULATION AND APPLICATION

Calculations of averaging kernels (AK) are carried out and applied to the AIRS-COSMIC differences for every matchup case. To solve the linearized forward problem,

$$(\vec{R} - \vec{R}_o) = \hat{K} (\vec{T}_{\text{true}} - \vec{T}_o),$$

where toa radiance and true atmospheric temperature are  $\vec{R}$  and  $\vec{T}_{\text{true}}$  with perturbations from them  $\vec{R}_o$  and  $\vec{T}_o$ , and the temperature Jacobian matrix  $d\vec{R}/d\vec{T}_{\text{true}}$  (of size number of spectral channels by number of atmospheric levels) is  $\hat{K}$ , a regularized inverse solution can be used as follows:

$$(\vec{T}_{\text{ret}} - \vec{T}_o) = \hat{A} (\vec{T}_{\text{true}} - \vec{T}_o)$$

$$\hat{A} = (\hat{K}'\hat{K} + \gamma\hat{I})^{-1} \times \hat{K}'\hat{K}$$

Here,  $\vec{T}_{\text{ret}}$  is the retrieved temperature,  $\hat{A}$  the averaging kernel,  $\gamma$  a constant, and  $\hat{I}$  the identity matrix. The minimum information approach is used, so for every month and latitude zone  $\gamma$  is determined so that it retains 99 percent of the information. This is done by applying singular value decomposition on the inverted matrix,  $\hat{K}'\hat{K}$ . Averaging kernels are then calculated using the AIRS temperature computed Jacobians for every matchup

case using the appropriate gamma value. To apply the AK to the AIRS – COSMIC differences, the following equation is used:

$$(\vec{T}_{ret} - \vec{T}_{true})_{smoothed} = (\vec{T}_{ret} - \vec{T}_o) - \hat{A} \times (\vec{T}_{true} - \vec{T}_o)$$

where  $\vec{T}_{ret}$  is defined to be the AIRS temperature profile,  $\vec{T}_{true}$ , at a higher vertical resolution, is defined to be the COSMIC temperature, and  $\vec{T}_o$  is also defined to be AIRS since the AIRS temperature profile is used to compute the Jacobian (Rodgers and Connor, 2003).

Figure 13 shows an example AIRS temperature Jacobian, or weighting function, for the AFGL mid-latitude winter temperature profile for the set of channels analyzed in this study. Dots indicate weighting function (WF) maxima that occur at ~1hPa and ~35hPa for the channels of  $667.5307\text{cm}^{-1}$  and  $666.774\text{cm}^{-1}$  respectively, which will be a main focus in later analyses. The WF illustrates the portion of the temperature profile represented by each radiance measurement (Rodgers, 1976). More centrally located within the carbon dioxide band, the channels with WFs peaking higher in the stratosphere yield a larger change in radiance for a given change in temperature than the channels with WFs peaking lower in the stratosphere. Fig 14 shows the computed averaging kernel for the associated temperature Jacobian of Fig 13 and illustrates the smoothing that a temperature retrieval from the measured AIRS radiances induces. The width of each curve is a measure of the vertical resolution of the AIRS observing system (Rodgers, 1976).

#### IV. STATISTICS

In following analyses, statistics are calculated on monthly or seasonal time scales and for 5 zonal bins with the exception of Sub-section 6c where 5-degree latitude zones

are used. The 5 zonal bins span 30 degrees, except for the tropical bin, which spans  $\pm 30^\circ\text{N}$ . Global statistics are computed from area weightings of the 5 zonal bins.

Time series shown are first resampled to a frequency of 12 times per day. Boxcar filters of length 12 and 360 are then passed over the data to obtain daily and approximately monthly averaged data.

### **B. CASE STUDY MATCHUPS**

Case study matchups of IR, RO, and radiosondes are included to help exemplify various characteristics of the data. The first matchup case was obtained over Madison on 4 November 2012 by launching a Vaisala radiosonde from the Atmospheric, Oceanic, and Space Sciences building within an hour's time of an Aqua and Suomi NPP overpass and a predicted COSMIC profile whose perigee point was located 100km to the northeast. A map of the sonde profile, COSMIC profile, and AIRS and CrIMSS retrievals averaged to create the raypath-averaged matchup profiles are shown in the top panel of Fig 15. The bottom panel of Fig 15 shows overlaid temperature profiles including two versions of the COSMIC temperature, the v2013 being the most recent after a hemispheric bias had been corrected for, and the ERA-Interim after interpolation to the COSMIC profile. The RO profile clearly has more vertical structure than the IR sounder profiles. For this case the RO is also better able to capture the tropopause structure. Above  $\sim 5$  hPa, the two different versions of COSMIC data are seen to diverge, giving light on the possible magnitude of RO structural uncertainty due to different processing methods. Larger differences between matchup temperatures are seen to occur around 1hPa as well as the surface region where the RO dry temperature displays the cold water vapor bias.

The second matchup case consists of a COSMIC, AIRS ray-path average, and ARM radiosonde profile from the Tropical West Pacific ARM site on 24 December 2010. Overlaid temperatures are seen in Fig 16. Again, COSMIC is seen to display finer vertical structures than the AIRS IR profile, and the largest differences between AIRS and COSMIC occur in the higher stratospheric regions. Fig 16's bottom panel illustrates how COSMIC is strikingly able to pick up the fine, oscillatory tropopause feature, most likely caused by the presence of tropical inertia gravity waves, that the AIRS profile smooths over.

### **C. RADIATIVE TRANSFER MODEL PERTURBATION STUDY**

To quantify the sensitivity of the computed radiances to the OSS input carbon dioxide and temperature two perturbation studies are performed. The carbon dioxide perturbation study input variations are shown in Figure 17's left panel. The control case is the January 2007, 44-46°N zonal mean CT CO<sub>2</sub> estimate while the input variations depicted as red and blue lines represent monthly 2-degree zonal maximum and minimum values respectively. These variations are used to assess errors in using the mean zonal CO<sub>2</sub> value in the matchup forward calculation input. The blue and black dashed lines of Fig 17's left panel depict constant with height input variations defined by the mean UTLS and mean surface CO<sub>2</sub> values respectively. Using a constant with height CO<sub>2</sub> profile defined by a single mean value can be an attractive simplification in the forward calculation process, and these two cases aim to assess possible error in using such estimates.

The resulting percent changes in the temperature Jacobian shown in the right panel of Fig 17 illustrate that sensitivity of the radiances to carbon dioxide is located

primarily below 100hPa. Corresponding computed brightness temperatures and the perturbation minus control BT differences are seen in Fig 18. The constant with height surface value perturbation produces changes in BT of up to 0.25K, while all other cases for all channels produce less than 0.01K differences. Potential error incurred due to using a zonally averaged CO<sub>2</sub> profile rather than a 3x2 degree profile is seen to be less than 0.01K for all channels—supporting the simplification of using zonally averaged CO<sub>2</sub> profiles.

The perturbation study of input temperature aims to quantify the sensitivity of the radiances to two different phenomena. The first phenomenon is an artifact introduced into the input temperature profiles by the forward calculation methodology that was previously mentioned. When the input RO and IR temperature profiles are merged with the climatology, a discontinuity in the temperature profile is often introduced near the top-of-atmosphere at the locations where the input RO and IR profiles end. The exact height of the discontinuity varies with each matchup case but is primarily a function of the season and latitude zone. For COSMIC, the discontinuity occurs within the 0.34 – 0.13 hPa pressure level range, and because climatology is inserted into the AIRS profile where it is for the COSMIC profile, the discontinuity level for AIRS is the same. The COSMIC and AIRS discontinuity's magnitude globally over the 6-year time period ranges from -88 to 77K and -44 K to 65K respectively, have a 10.2K and 7.3K standard deviation, and have a mean of -7.6K and -9.3K. Fig 19's left and middle panels shows four perturbation cases that investigate this phenomenon's effect on the calculated BTs. The solid red line shows a perturbation case with a discontinuity whose vertical height of 0.34hPa and magnitude of 12K is determined by the mean January 2007 NH mid-latitude

COSMIC input temperature discontinuity. Variations of opposite magnitude (blue line) and with different height locations (red dashed and dotted) are also shown. The perturbation at 0.13hPa represents the highest location that discontinuities take place while the 0.34hPa represents the lowest location.

The second phenomenon investigated in the temperature perturbations study is that of a mean temperature bias seen between UCAR's previous COSMIC and GRAS versions. The GRAS minus COSMIC RO bias is discussed in greater detail in Feltz et al. (2014b) and is largest in the stratosphere. A perturbation with the Jan 2007 NH GRAS minus COSMIC bias as detected by a double difference from IASI is performed and is illustrated as the black dashed line in Fig. 19's right and left panel.

The resulting sensitivities of the temperature Jacobians to the varied input temperatures are seen in the right panel of Fig 19 as percent differences. The RO bias produces the smallest percent change, while as could be expected, the lowest in height positive temperature discontinuity changes the temperature Jacobian at the lowest heights. The highest discontinuity produces Jacobian changes that are largest in magnitude, but the changes are confined to higher altitudes. Corresponding computed BTs and control minus perturbation BT differences are shown in Fig 20. As the height of the temperature discontinuity decreases, the change in BT for all channels increases. Table 2 shows the change in brightness temperature per 1K change in magnitude of the 0.34hPa temperature discontinuity. While the significance of a BT uncertainty varies with the context of the analysis, the  $666.7\text{cm}^{-1}$  channel, 0.34hPa temperature discontinuity 0.0074K/K effect is primarily negligible in this study due to the fact that the AIRS measured radiance uncertainty is 0.5K; thus, a 67K (outside of the 3 sigma range)

temperature discontinuity at 0.34hPa is necessary for the computed BT discontinuity effect to be equivalent to the AIRS measured BT uncertainty. In contrast, the  $667.5\text{cm}^{-1}$  channel is much more sensitive to the temperature discontinuity effect, experiencing a 0.1111K/K change, which would require a mere 4.5K magnitude discontinuity for the discontinuity effect to be larger than the AIRS measured uncertainty. This illustrates that channel selection is an important process. In later sections, adjusted calculated BT time series will be used that have the discontinuity effect removed. The removed effect is calculated by multiplying the magnitude of the temperature discontinuity by the sensitivity of the BT to the discontinuity effect (such as those seen in Table 2). The sensitivity used is that for the correct channel and for either the 0.34 or 0.13 hPa level—whichever one is that is closest in height to the discontinuity.

The BT change produced by the GRAS minus COSMIC bias is more consistent across channels and is confined below 1.5K. For certain channels, the change is large enough so that a theoretical comparison of forward calculated GRAS and COSMIC BTs to the AIRS measured BTs could enable a statistically significant difference. From this, it could be determined whether COSMIC or GRAS temperatures are more consistent with the AIRS measured BTs; however, this is outside the scope of this thesis.

#### **D. REVISITING MEAN AIRS – MEAN COSMIC: ELIMINATION OF SAMPLING DIFFERENCES**

Figures 21 and 22 show follow on analyses of Section 5c's mean AIRS – mean COSMIC result (Figs 4 and 10). Fig 21's and 22's results are obtained from the AIRS and COSMIC matchup dataset, which is a subset of the complete datasets analyzed previously with reduced temporal and horizontal spatial sampling errors. The matchup

dataset in Fig 21 shows similarity to the complete dataset in Fig 4, with only small differences being visible in the mean temperatures. For example, Fig 4's 35hPa AIRS-COSMIC difference map shows greater than 4K differences located around 2009 at 90°N while Fig 21's matchup analysis removes these structures. A comparison of the matchup and complete dataset histograms in Figs 22 and 10 again reveals that though the range of temperature differences is altered, the statistical measures are only slightly changed and great resemblance exists in both the global and tropical datasets. The similarity between the matchup and complete dataset results reveals that temporal and horizontal spatial sampling errors are not dominant contributors to the mean AIRS – mean COSMIC differences at these time and space scales. This is further supported by Table 3, which shows for various latitude regions the comparison of statistical measures of the monthly, zonal complete and matchup dataset AIRS-COSMIC temperature differences. Estimates of the mean difference in each zone are in agreement for the two comparison approaches within the estimated uncertainty.

Figure 23 shows the Tropics and Antarctic zonal time series of the AIRS-COSMIC matchup temperatures for the 1 and 35 hPa levels. Overlaid in each panel are differently filtered time series as well as a best-fit, 1-degree polynomial. While the resampled data highlights the seemingly chaotic sub-daily variations, the daily and approximately monthly filtered data more clearly suggest seasonal patterns where they occur, which could aid in determination of contributors to the AIRS-COSMIC difference. Though the magnitudes of the differences vary with height and latitude zone, being largest at 1hPa and in the Antarctic zone, the structure of the time series remains somewhat similar across the pressure levels (or throughout the height of the stratosphere),

with less periodicity in the Tropics. The best-fit one-degree polynomials show that the differences have an overall positive, temporally constant offset from zero in the Tropics, yielding a 0.0624K/yr and 0.0010 K/yr trend at 1hPa and 35hPa respectively. In the Antarctic zone a negative offset that grows more positive in time over the years shown is seen amounting to a 0.2169 K/yr and a 0.0879 K/yr trend at 1hPa and 35hPa respectively. While such a short time series of AIRS minus COSMIC matchup temperature differences cannot produce accurate long-term trend estimates, this result demonstrates the utility of comparing AIRS and COSMIC in such a manner for climate studies. If there is no drift found between RO and IR sounder products, greater confidence could be placed in the estimates of the trends independently recorded by each instrument. For example, more confidence could be placed in the AIRS and COSMIC temperature trends in the 35hPa Tropics zone where the AIRS-COSMIC time series shows no trend over the time period shown.

Even though this subsection introduced a COSMIC and AIRS matchup dataset with reduced sampling differences, another last step is needed to obtain an even more complete comparison of AIRS and COSMIC data. The fact that RO has a higher vertical resolution than IR sounders could be contributing to the differences in AIRS and COSMIC; therefore, a smoothing of the vertical scale is applied in the next subsection. Additionally, in following analyses 30-day filtered time series are presented to direct focus on the longer-term temperature variations.

#### **E. ADDRESSING DIFFERENCES IN VERTICAL RESOLUTION**

As described in the method section, vertically smoothed temperatures are obtained by applying calculated AIRS averaging kernels to the AIRS-COSMIC

differences. While in theory only vertical structure of the higher resolution COSMIC profiles should be removed, it has been shown that application of the AK to the AIRS temperature profiles alone can remove vertical structures due to artifacts introduced by the AIRS retrieval (Feltz et al., 2014b). Because structure can be removed from both the AIRS and COSMIC profiles, differences due to errors in the AIRS or COSMIC temperature profile products can be smoothed out and not show up in the smoothed difference. More specifically, the vertically smoothed temperature differences include only part and not all of the measurement and retrieval errors.

Figure 24 shows the 30-day filtered times series of vertically smoothed and non-smoothed AIRS-COSMIC temperature differences for the 1 and 35 hPa levels and various latitude zones. (Note the change of scale between the 1 and 35hPa figures.) In general, for all zones and levels, vertical smoothing decreases the AIRS-COSMIC difference. The difference is reduced the most in the Antarctic latitude zone during the months of Feb. to June, where the AIRS ‘vertical oscillation error’ is known to be—the difference is reduced by up to 3K at 1hPa and up to 1K at 35hPa. Comparing the SH and NH polar temperature differences reveals a somewhat opposing periodic, seasonal structure at both levels between the two hemispheres with the exception of the NH spikes in the differences around periods of sudden stratospheric warmings in the wintertime months.

#### **F. COMPARISONS IN RADIANCE AND TEMPERATURE SPACE**

In this section AIRS and COSMIC calculated BTs are compared to AIRS measured BTs which have an estimated absolute accuracy of less than  $\sim 0.5\text{K}$ . These

analyses provide a method for determining whether AIRS, COSMIC, or both have errors that are contributing to the AIRS-COSMIC smoothed temperature difference.

Figures 25 and 26 show overlaid 30-day filtered BT and temperature difference time series for 2 pressure levels/channels with global and all 5 latitude zones shown. The  $\sim 1\text{hPa}$  level temperatures are overlaid with the  $667.5\text{cm}^{-1}$  channel BTs, whose weighting function peaks around 1hPa, and similarly the  $\sim 35\text{hPa}$  temperature and  $666.7\text{cm}^{-1}$  BTs are overlaid. Adjusted calculated minus measured BT time series that have the temperature discontinuity effect removed as discussed in detail in subsection 6c are included. In general, the AIRS BT differences have much less seasonal structure than the COSMIC BT differences. The AIRS calculated BTs are in better agreement with the measured BTs with the exception of the Tropics and Mid-Latitudes at 1hPa, which should be expected due to the fact that AIRS temperature retrievals ought to be constrained to satisfy the measurements. At 35hPa the AIRS BT differences are within the 0.5K measurement uncertainty. The COSMIC BT differences have a qualitatively similar structure to the smoothed temperature differences (note the difference is flipped from previous analyses for easier comparison purposes), and at 35hPa they are also generally the same magnitude as the smoothed temperature differences. This suggests that the COSMIC temperatures are the dominating contributor to the *smoothed* temperature difference. The overall largest differences occur in the COSMIC BT and smoothed temperature differences, and for both pressure levels, are located in the polar regions. The COSMIC-AIRS temperature difference is close to zero during polar summer but COSMIC is significantly warmer than AIRS during the polar winters—by over 1K at 35hPa and over 10K at 1hPa. (X-axis year tick marks are centered on July 1<sup>st</sup>.) Where BT

differences are greater than 0.5K at the 35hPa level, there can be confidence placed in fact that corresponding temperatures contain errors. Due to methodological uncertainties, no conclusions about the 1hPa level are made here.

Figures 27 and 28 show zonal adjusted BT differences as a function of height as well as the COSMIC minus AIRS vertically smoothed and non-smoothed temperatures for the DJF and JJA season respectively. The BT differences are plotted at heights where each channel's weighting function peaks and are overlaid with horizontal and vertical error bars that represent their mean uncertainty and the channels' WFs full widths at half max respectively. The tropical BT difference results are seen to be quite similar across the DJF and JJA seasons, but other zones' difference characteristics vary with season, which potentially could aid in the determination of error sources. AIRS BT differences are generally within the 0.5K uncertainty range below 3hPa with the exception being the JJA Antarctic zone. AIRS BTs transition from being slightly cooler than the measured BTs below the ~3hPa level to being warmer above. COSMIC BTs also become increasingly warmer than the measured BTs with height, most drastically in the polar zones. For channels whose WFs peak around 30hPa, where highest confidence is placed in the BT calculations, COSMIC BTs are generally within the estimated AIRS measurement uncertainty of 0.5K with the exception of the JJA Antarctic and both DJF polar zones where they are within 1K. While one should still be careful to interpret the results at higher levels due to the forward calculation methodologies, above ~5 hPa the COSMIC BTs diverge more significantly from the BT measurements, which is consistent with ideas in current literature that RO is most accurate in the UTLS range but is vulnerable to increasing initialization and ionospheric errors above.

Lastly, Figure 29 shows monthly, 5-degree zonally averaged maps of the BT differences for the  $666.774\text{cm}^{-1}$  channel, whose WF peaks at  $\sim 35\text{hPa}$ . In comparison to the  $\sim 35\text{hPa}$  seasonal and large latitude bin averaged differences shown in the previous figures, the BT differences seen on these scales are larger. AIRS BT difference magnitudes are dominantly under  $0.5\text{K}$  while COSMIC's are often above  $1\text{K}$ , sometimes above  $3\text{K}$  in the polar region wintertime. COSMIC BTs are warmer than the measured BTs in the early winter months. Both AIRS and COSMIC calculated BTs are cooler than the measured BTs in the tropical regions. The patterns of errors seen for both instruments motivate the idea that zonal latitudinal analyses should be carried out when validating satellite temperature products. By using global averages over larger time scales, characteristics of errors that could aid in the determination of their sources can be masked.

## 7. DISCUSSION

In this section the previous results are discussed and interpreted in the context of the methodologies employed in this study. To begin, it is seen that differences of AIRS and COSMIC complete dataset temperatures reveal characteristic patterns in space and time and reach over 10K in the stratosphere on monthly, 5-degree zonal scales.

Application of the temperature profile matchup method and calculated averaging kernels indicates that the majority of the AIRS and COSMIC temperature differences throughout the stratosphere are the not the product of the differences in instrument sampling in time and space or vertical resolution, but rather, they are a product of differences in retrieval errors. Thus, the use of the restricted matchup dataset has the same statistical properties of the full dataset but has the advantage of being able to make one-to-one profile comparisons against coincident radiance observations. Vertical smoothing of the AIRS-COSMIC difference is applied to remove the effect of the vertical resolution differences, however, this also removes vertical structures present in both the AIRS and COSMIC temperature profiles that could be due to retrieval and measurement errors. Vertical smoothing can reduce the AIRS-COSMIC matchup differences on monthly, seasonal zonal averaged scales by over 3K in the upper stratosphere and by over 1K in the lower stratosphere. Temperature smoothing has the largest effect in polar regions.

In the calculation of brightness temperatures from the AIRS and COSMIC temperature profiles, the methodology used proves to be an essential consideration. Perturbation studies show for carbon dioxide input that the use of a monthly 2-degree zonal averaged profile can improve upon the calculated BT by up to 0.25K in comparison to the use of a constant with height profile based off of a surface estimate. Thus the CO<sub>2</sub>

uncertainties can be minimized in the forward calculated radiances. The temperature discontinuity introduced by attaching a zonal climatology above the top of the COSMIC or AIRS temperature profile has the largest effect on the  $667.5307\text{-}668.4524\text{ cm}^{-1}$  channels whose weighting functions peak in the upper stratosphere, while it has a potentially negligible effect on other channels such as the  $666.7740\text{ cm}^{-1}$  whose WFs peak in the lower stratosphere. Unfortunately, this makes it challenging to interpret results obtained by the methodology used in this paper. Because AIRS and COSMIC temperature profiles are treated in the same way in terms of where climatology is added, an equal amount of error due to this issue should be present in their calculated BTs. Thus a comparison of the AIRS and COSMIC BTs, or in this case the AIRS calculated minus AIRS measured and the COSMIC calculated minus AIRS measured differences would yield substantial insight in terms of how they compare to each other. Interestingly, Figures 27 and 28 show that the difference between the calculated BTs, or the equivalence of the AIRS calculated minus COSMIC calculated BTs, is often the same sign and a similar magnitude as the corresponding AIRS minus COSMIC temperatures.

In comparing COSMIC and AIRS calculated BTs to the AIRS measured BT reference, however, treatment of the input temperature profiles has a larger ability to offer misleading results for channels with higher peaking WFs. Thus, results for the  $667.5307\text{ cm}^{-1}$  channel are shown as preliminary and ought to be improved upon. While the adjustment performed in this study is limited in its use of a single sensitivity (the BT K/Temp K) from one atmospheric state, i.e. the mid-latitude winter, it offers a technique for gaining insight on where and at what general magnitude the temperature discontinuity effect takes place. The discontinuity effect calculated here has an influence of less than

0.1K on the  $666.7\text{cm}^{-1}$  BT channel and less than 2K on the  $667.5\text{cm}^{-1}$  channel for monthly averages. Thus, confidence might be placed in the interpretation that COSMIC has a warm bias that is most dramatic in polar wintertime in the upper stratosphere and is in good agreement with AIRS measured BTs for channels with lower stratospheric peaking WFs. However, the larger AIRS calculated and measured BT disagreement at higher altitudes above 0.3hPa, where the discontinuity effect is strongest, suggests that the treatment of the input temperature profile still affects the adjusted BTs. Even a comparison of AIRS BTs calculated using the best forward calculation method with the measured BTs would still only offer a consistency check, and could not be expected to reveal null space errors in the AIRS temperature profile. For example, AIRS calculated JJA Antarctic BTs are shown to not be far from agreement with the measured radiances, but knowledge from previous analyses indicates the presence of large vertical oscillation errors in corresponding AIRS temperature profiles.

The methods applied in the study instruct changes that could improve the strength of the forward calculated results in planned future work. For example, another choice for the treatment of the temperature profiles would be to extrapolate the profiles or shift the climatology portion of the profile to be in line with AIRS and COSMIC temperature profile portion so that no discontinuity is present.

## 8. CONCLUSIONS

Upon interpretation of the comparison of COSMIC and AIRS temperature and forward calculated brightness temperature datasets, conclusions can be drawn about their potential use in monitoring stratospheric temperatures. In regards to IR sounder and RO sampling characteristic adequacy for climate studies, complete dataset analyses showed both AIRS and COSMIC have sufficient sampling coverage for monthly and 5° latitude zonal scales. An exception is granted for regions directly over the poles for AIRS.

The adequacy of current RO and IR sounder temperature profile product accuracy was found to be lacking within stratospheric regions. AIRS products were shown to contain unphysical characteristics in specific stratospheric regions, markedly the Antarctic winter, on monthly, zonal scales. COSMIC calculated BTs showed seasonally dependent errors of significant, over 2K magnitudes in the upper stratosphere on seasonal, zonal scales. A COSMIC warm bias that grows with height in the stratosphere is implied by the results of this thesis and is consistent with current literature's knowledge that RO is most accurate in the UTLS but accumulates errors above due to ionospheric contributions. A study done by Das et al. (2014) that compares COSMIC and SABER temperatures from Dec 2010 – Nov 2011 provides stimulating comparisons (see Das et al. Fig 2). Like the COSMIC BT differences, Das et al. (2014) finds that COSMIC dry temperatures for all seasons and zones also transition from being cooler than their reference, SABER, to being warmer at around 1-5hPa, being ~2K cooler below and over 5K warmer above at ~0.3hPa. However, while Das et al. (2014) concludes, "COSMIC data can be used with confidence up to 1hPa," results shown here caution the use of COSMIC data for certain seasons and latitude zones at lower altitudes—though it is

recognized that the necessary degree of accuracy varies with the analysis being performed. Another recent study that yields an interesting comparison opportunity is that of Ladstädter et al. (2015) which compares multiple radiosonde datasets to RO data from 3 different missions (see Figure 4 of Ladstädter et al. (2015)). Ladstädter et al. (2015) finds that over the coincident time period of this study that global, annual RO differences from radiosondes in both the 30-100hPa and the 30-10hPa layer are mostly positive, having a rough upper bound at 0.3K, with the higher stratospheric layer having larger magnitude differences. Global, monthly time series of COSMIC and AIRS differences show qualitatively similar results.

While results shown motivate future work on making AIRS and COSMIC temperature products more accurate for certain latitude zones and time periods, specifically polar regions, it also demonstrates the potential use for RO and IR sounders in monitoring stratospheric temperatures. The hyperspectral infrared sounder and radio occultation instruments have been shown to offer measurements amenable for climate studies and work continues to be done on improving the derived temperature products, though it is not yet complete (Wee and Kuo, 2014). Future retrievals for the CrIS and IASI sounders should include improvements within stratospheric regions and throughout the polar zones. Work should continue to be done as well on RO processing for stratospheric temperatures and better characterization of ionospheric contributions.

**APPENDIX A: ACRONYMS**

ACRONYM	NAME
AIRS	Atmospheric Infrared Sounder
AMSU	Advanced Microwave Sounding Unit
CLARREO	Climate Absolute Radiance and Refractivity Observatory
CLASS	Comprehensive Large Array-Data Stewardship System
COSMIC	Constellation Observing System for Meteorology, Ionosphere & Climate
CrIMSS	Cross-Track Infrared and Microwave Sounder Suite
CrIS	Cross-Track Infrared Sounder
ECMWF	European Center for Medium-Range Weather Forecasting
GCOS	Global Climate Observing System
GNSS	Global Navigation Satellite System
GPS	Global Positioning System
GRAS	GNSS Receiver for Atmospheric Sounding
IASI	Infrared Atmospheric Sounding Interferometer
IPCC	Intergovernmental Panel on Climate Change
JPSS	Joint Polar Satellite System
JRA-55	Japan Reanalysis 55 Years
MERRA	Modern Era Retrospective-Analysis for Research
MSU	Microwave Sounding Unit
NASA	National Aeronautics and Space Administration
NOAA	National Oceanic and Atmospheric Administration
NPP	National Polar-orbiting Partnership
SSU	Stratospheric Sounding Unit
UCAR	University Corporation for Atmospheric Research
UTLS	Upper Troposphere-Lower Stratosphere
WMO	World Meteorological Organization

## REFERENCES

- Anthes, Richard A., et al. "The COSMIC/FORMOSAT-3 mission: Early results." *Bulletin of the American Meteorological Society* 89.3 (2008): 313-333.
- Aumann, Hartmut H., et al. "AIRS/AMSU/HSB on the Aqua mission: Design, science objectives, data products, and processing systems." *Geoscience and Remote Sensing, IEEE Transactions on* 41.2 (2003): 253-264.
- Berrisford, Paul, et al. "Atmospheric conservation properties in ERA-Interim." *Quarterly Journal of the Royal Meteorological Society* 137.659 (2011): 1381-1399.
- Danzer, Julia, Barbara Scherllin-Pirscher, and Ulrich Foelsche. "Systematic residual ionospheric errors in radio occultation data and a potential way to minimize them." *Atmospheric Measurement Techniques* 6.8 (2013): 2169-2179.
- Das, U., and C. J. Pan. "Validation of FORMOSAT-3/COSMIC level 2" atmPrf" global temperature data in the stratosphere." *Atmospheric Measurement Techniques* 7.3 (2014): 731-742.
- Dee, D. P., et al. "The ERA-Interim reanalysis: Configuration and performance of the data assimilation system." *Quarterly Journal of the Royal Meteorological Society* 137.656 (2011): 553-597.
- Divakarla, Murty, et al. "The CrIMSS EDR algorithm: Characterization, optimization, and validation." *Journal of Geophysical Research: Atmospheres* 119.8 (2014): 4953-4977.
- Feltz, Michelle L., et al. "A methodology for the validation of temperature profiles from hyperspectral infrared sounders using GPS radio occultation: Experience with AIRS and COSMIC." *Journal of Geophysical Research: Atmospheres* 119.3 (2014a): 1680-1691.
- Feltz, M., et al. "Application of GPS radio occultation to the assessment of temperature profile retrievals from microwave and infrared sounders." *Atmospheric Measurement Techniques* 7.11 (2014b): 3751-3762.
- Foelsche, Ulrich, et al. "Observing upper troposphere–lower stratosphere climate with radio occultation data from the CHAMP satellite." *Climate dynamics* 31.1 (2008): 49-65.
- Foelsche, U., et al. "Errors in GNSS radio occultation data: relevance of the measurement geometry and obliquity of profiles." *Atmospheric Measurement Techniques* 4.2 (2011a): 189-199.
- Foelsche, U., et al. "Refractivity and temperature climate records from multiple radio occultation satellites consistent within 0.05%." *Atmospheric Measurement Techniques* 4.9 (2011b): 2007-2018.
- Foelsche, Ulrich. "On possible reasons for systematic errors in GPS radio occultation climatologies, their characterization, and potential ways to remove some of them." Eighth FORMOSAT-3/COSMIC Data Users' Workshop. UCAR Center Green Campus, Boulder, CO. 02 Oct 2014. Conference Presentation.
- Gaffen, Dian J. "Temporal inhomogeneities in radiosonde temperature records." *Journal of Geophysical Research: Atmospheres* (1984–2012) 99.D2 (1994): 3667-3676.
- GCOS, "Systematic Observation Requirements for Satellite-Based Data Products for Climate." WMO Tech. Doc. GCOS-154. 21. (2011)

- Haimberger, Leopold, Christina Tavalato, and Stefan Sperka. "Toward elimination of the warm bias in historic radiosonde temperature records-Some new results from a comprehensive intercomparison of upper-air data." *Journal of Climate* 21.18 (2008): 4587-4606.
- He, Wenying, et al. "Assessment of radiosonde temperature measurements in the upper troposphere and lower stratosphere using COSMIC radio occultation data." *Geophysical Research Letters* 36.17 (2009).
- Ho, Shu-peng, et al. "Estimating the uncertainty of using GPS radio occultation data for climate monitoring: Intercomparison of CHAMP refractivity climate records from 2002 to 2006 from different data centers." *Journal of Geophysical Research: Atmospheres* (1984–2012) 114.D23 (2009).
- Ho, S.-P., et al. "Reproducibility of GPS radio occultation data for climate monitoring: Profile-to-profile inter-comparison of CHAMP climate records 2002 to 2008 from six data centers." *Journal of Geophysical Research*. 117.D18. (2012). doi:10.1029/2012JD017665.
- Hoffmann, L., and M. J. Alexander. "Retrieval of stratospheric temperatures from Atmospheric Infrared Sounder radiance measurements for gravity wave studies." *Journal of Geophysical Research: Atmospheres* (1984–2012) 114.D7 (2009).
- JPSS Configuration Management Office: Joint Polar Satellite System (JPSS) Algorithm Theoretical Basis Document For the Cross Track Infrared Sounder (CrIS) Volume II, Environmental Data Records (EDR), JPSS office, document code 474: 474-00056, available at: <http://npp.gsfc.nasa.gov/documents.html> (last access: 04 June 2014), 2012.
- Kursinski, E. R., et al. "Observing Earth's atmosphere with radio occultation measurements using the Global Positioning System." *Journal of Geophysical Research: Atmospheres* (1984–2012) 102.D19 (1997): 23429-23465.
- Ladstädter, Florian, et al. "Climate comparison of reference upper-air measurements: GPS radio occultation and GRUAN radiosondes." *EGU General Assembly Conference Abstracts*. Vol. 17. 2015.
- Leroy, Stephen S., John A. Dykema, and James G. Anderson. "Climate benchmarking using GNSS occultation." *Atmosphere and Climate*. Springer Berlin Heidelberg, 2006. 287-301.
- Liu, X., et al. "Retrieving atmospheric temperature and moisture profiles from SUOMI NPP CrIS/ATMS sensors using CrIMSS EDR algorithm, Geoscience and Remote Sensing Symposium (IGARSS)." 2012 IEEE International. (2012):1956-1959. doi:10.1109/IGARSS.2012.6350816.
- Mannucci, A. J., Ao, C. O., Yunck, T. P., Young, L. E., Hajj, G. A., Iijima, B. A., Kuang, D., Meehan, T. K., and Leroy, S. S.: Generating climate benchmark atmospheric soundings using GPS occultation data, Proc. SPIE 6301, Atmospheric and Environmental Remote Sensing Data Processing and Utilization II: Perspective on Calibration/Validation Initiatives and Strategies. 630108. (2006) doi:10.1117/12.683973.
- Mannucci, A. J., et al. "The impact of large scale ionospheric structure on radio occultation retrievals." *Atmospheric Measurement Techniques* 4.12 (2011): 2837-2850.

- Moncet, Jean-Luc, et al. "Infrared radiance modeling by optimal spectral sampling." *Journal of the Atmospheric Sciences* 65.12 (2008): 3917-3934.
- Nalli, Nicholas R., et al. "Validation of satellite sounder environmental data records: Application to the Cross-track Infrared Microwave Sounder Suite." *Journal of Geophysical Research: Atmospheres* 118.24 (2013): 13-628.
- Peters et al. "An atmospheric perspective on North American carbon dioxide exchange: CarbonTracker." *PNAS*. November 27, 2007. 104.48. (2007):18925-18930.
- Philipona, R., et al. "Solar and thermal radiation errors on upper-air radiosonde temperature measurements." *Journal of Atmospheric and Oceanic Technology* 30.10 (2013): 2382-2393.
- Randel, William J., et al. "An update of observed stratospheric temperature trends." *Journal of Geophysical Research: Atmospheres* (1984–2012) 114.D2 (2009).
- Rodgers, Clive D. "Retrieval of atmospheric temperature and composition from remote measurements of thermal radiation." *Reviews of Geophysics* 14.4 (1976): 609-624.
- Rodgers, Clive D., and Brian J. Connor. "Intercomparison of remote sounding instruments." *Journal of Geophysical Research: Atmospheres* (1984–2012) 108.D3 (2003).
- Seidel, Dian J., et al. "Stratospheric temperature trends: Our evolving understanding." *Wiley Interdisciplinary Reviews: Climate Change* 2.4 (2011): 592-616.
- Shine, Keith P., John J. Barnett, and William J. Randel. "Temperature trends derived from Stratospheric Sounding Unit radiances: The effect of increasing CO<sub>2</sub> on the weighting function." *Geophysical Research Letters* 35.2 (2008).
- Simmons, A. J., et al. "Estimating low-frequency variability and trends in atmospheric temperature using ERA-Interim." *Quarterly Journal of the Royal Meteorological Society* 140.679 (2014): 329-353.
- Steiner, A. K., et al. "GPS radio occultation for climate monitoring and change detection." *Radio Science* 46.6 (2011).
- Steiner, A. K., et al. "Quantification of structural uncertainty in climate data records from GPS radio occultation." *Atmospheric Chemistry and Physics* 13.3 (2013): 1469-1484.
- Strow, L. Larrabee, et al. "An overview of the AIRS radiative transfer model." *Geoscience and Remote Sensing, IEEE Transactions on* 41.2 (2003): 303-313.
- Sun, Bomin, et al. "Comparing radiosonde and COSMIC atmospheric profile data to quantify differences among radiosonde types and the effects of imperfect collocation on comparison statistics." *Journal of Geophysical Research: Atmospheres* (1984–2012) 115.D23 (2010).
- Sun, Bomin, et al. "Toward improved corrections for radiation-induced biases in radiosonde temperature observations." *Journal of Geophysical Research: Atmospheres* 118.10 (2013): 4231-4243.
- Susskind, Joel, Christopher D. Barnet, and John M. Blaisdell. "Retrieval of atmospheric and surface parameters from AIRS/AMSU/HSB data in the presence of clouds." *Geoscience and Remote Sensing, IEEE Transactions on* 41.2 (2003): 390-409.

- Susskind, Joel, et al. "Improved temperature sounding and quality control methodology using AIRS/AMSU data: The AIRS science team version 5 retrieval algorithm." *Geoscience and Remote Sensing, IEEE Transactions on* 49.3 (2011): 883-907.
- Syndergaard, Stig. "On the ionosphere calibration in GPS radio occultation measurements." *Radio Science* 35.3 (2000): 865-883.
- Thompson, David WJ, et al. "The mystery of recent stratospheric temperature trends." *Nature* 491.7426 (2012): 692-697.
- Tobin, David, et al. "Suomi-NPP CrIS radiometric calibration uncertainty." *Journal of Geophysical Research: Atmospheres* 118.18 (2013): 10-589.
- Wang, Likun, Cheng-Zhi Zou, and Haifeng Qian. "Construction of stratospheric temperature data records from stratospheric sounding units." *Journal of Climate* 25.8 (2012): 2931-2946.
- Wee, Tae-Kwon, and Ying-Hwa Kuo. "Advanced stratospheric data processing of radio occultation with a variational combination for multifrequency GNSS signals." *Journal of Geophysical Research: Atmospheres* 119.19 (2014): 11-011.
- Young, Paul J., et al. "The seasonal cycle and interannual variability in stratospheric temperatures and links to the Brewer-Dobson circulation: An analysis of MSU and SSU data." *Journal of Climate* 24.23 (2011): 6243-6258.
- Yulaeva, Elena, James R. Holton, and John M. Wallace. "On the cause of the annual cycle in tropical lower-stratospheric temperatures." *Journal of the atmospheric sciences* 51.2 (1994): 169-174.

## TABLES

Table 1. Forward Calculation Input

OSS Model Parameter	Source
Pressure Profile	AIRS 101 Product levels
Top of Atmosphere Pressure	1.0E-3 hPa
Surface Pressure	ERA-Interim 6-hrly, 0.75° gridded closest to matchup location
Skin Temperature	ERA-Interim 6-hrly, 0.75° gridded closest to matchup location
Water Vapor Profile	CDAAC COSMIC 'eraPrf' files - ERA-Interim profile interpolated to COSMIC profile location by CDAAC processing
Carbon Dioxide Profile	CarbonTracker monthly 2° zonal averages
Ozone Profile	ERA-Interim 6-hrly, 0.75° gridded closest to matchup location
Slant Angle	Mean AIRS sensor view angle of AIRS L1B 3x3 golfball that corresponds to single L2 retrieval FOV
Solar Zenith Angle	90 degrees, nadir

Table 2. Estimated calculated BT uncertainty per 1 K temperature discontinuity at 1hPa from 0.34hPa 12K temperature discontinuity perturbation run

<b>Calculated Brightness Temperature Sensitivity to Temperature Discontinuity Effect at 0.34hPa</b>	
<b>Channel (cm<sup>-1</sup>)</b>	<b>BT K/ Temperature K</b>
<b>666.7740</b>	<b>0.0074</b>
667.0260	0.0063
667.2783	0.0545
<b>667.5307</b>	<b>0.1111</b>
667.7833	0.1314
668.0361	0.1251
668.2892	0.0985
668.5424	0.0686
668.7958	0.0484
669.0495	0.0388
669.3033	0.0322
669.5574	0.0322
669.8116	0.0329
671.0859	0.0165
671.3414	0.0213
671.8530	0.0083
672.1091	0.0050

Table 3. Statistical measures of the 35hPa level monthly, 5-degree zonally averaged complete and matchup dataset AIRS minus COSMIC temperatures differences for different latitude zones in Kelvin.

Latitude	Complete Dataset			Matchup Dataset		
	Mean	Stdev.	Mean Unc.	Mean	Stdev.	Mean Unc.
90N-90S	-0.022061	0.94483	0.018558	-0.036028	0.92521	0.018173
90N-60N	-0.4799	0.94241	0.045342	-0.59692	0.68448	0.032932
60N-30N	-0.19119	0.40645	0.019555	-0.15895	0.39053	0.018789
30N-30S	0.80417	0.44781	0.015235	0.82413	0.47874	0.016287
30S-60S	-0.12383	0.39806	0.019152	-0.11157	0.40708	0.019586
60S-90S	-0.94579	1.1315	0.05444	-0.99699	1.0749	0.051716

**FIGURES**

Fig 1. 1 January 2007 COSMIC tangent point locations (top) and AIRS 1x1 degree gridded product counts (bottom).

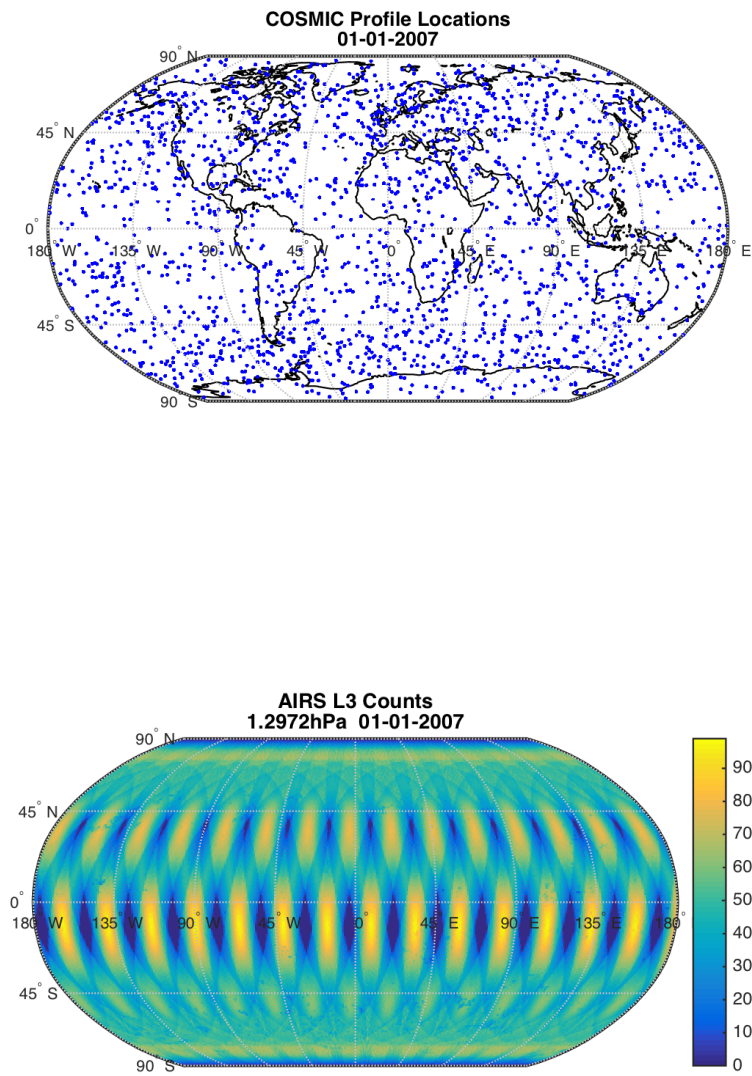


Fig 2. Monthly, 5° zonal number of samples at ~1hPa for COSMIC (top, contoured by 500 counts) and AIRS (bottom, contoured by 5E5 counts). Year tick marks for this and all subsequent plots are centered on July 1<sup>st</sup>.

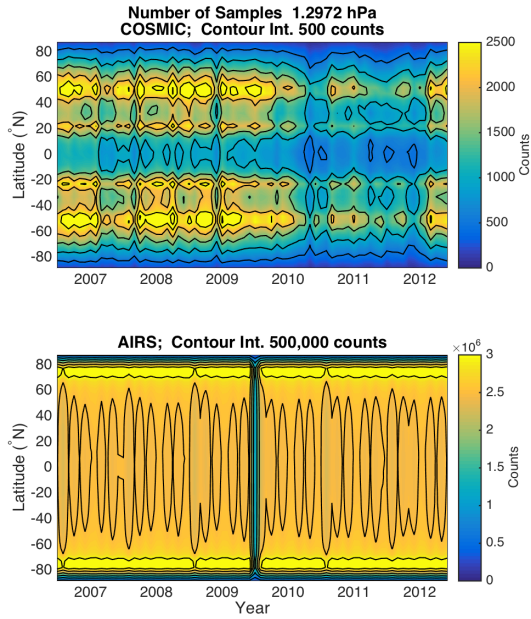


Fig 3. Monthly, 5° zonal standard deviation at ~1hPa (left) and ~35hPa (right) for COSMIC (top) and AIRS (bottom) contoured by 10K (bold) and 5K (thin).

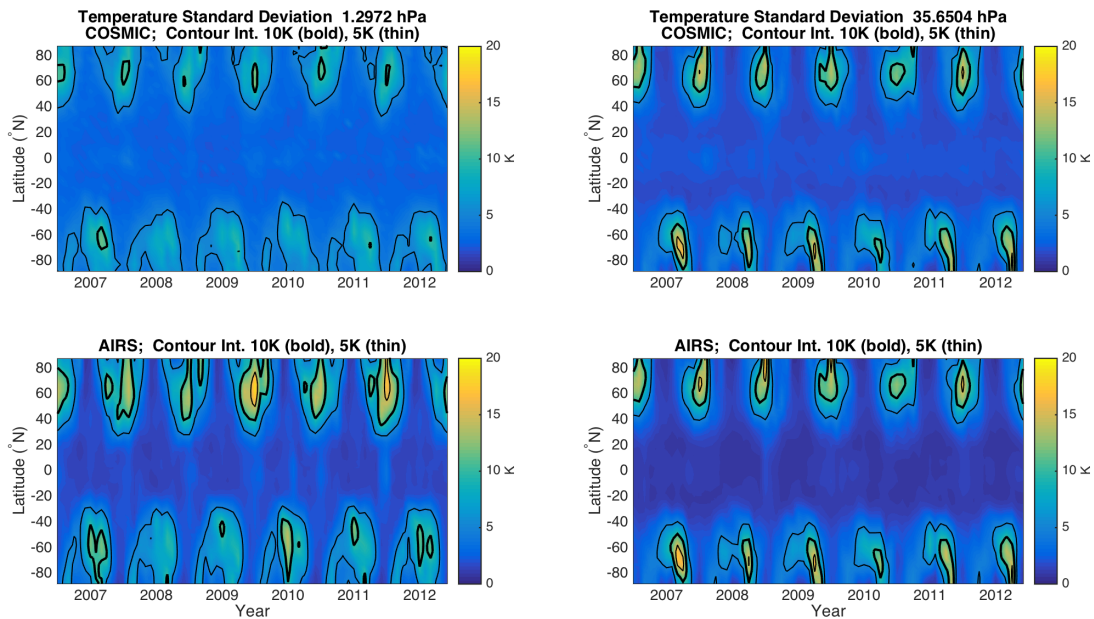


Fig 4. Monthly, 5° zonal ~1hPa (left) and ~35hPa (right) COSMIC mean temperature (top, contoured bold every 10K and thin every 5K), AIRS mean temperature (middle, contoured bold every 10K and thin every 5K), and mean AIRS minus mean COSMIC difference (bottom, contoured bold at 0K and thin every 2K).

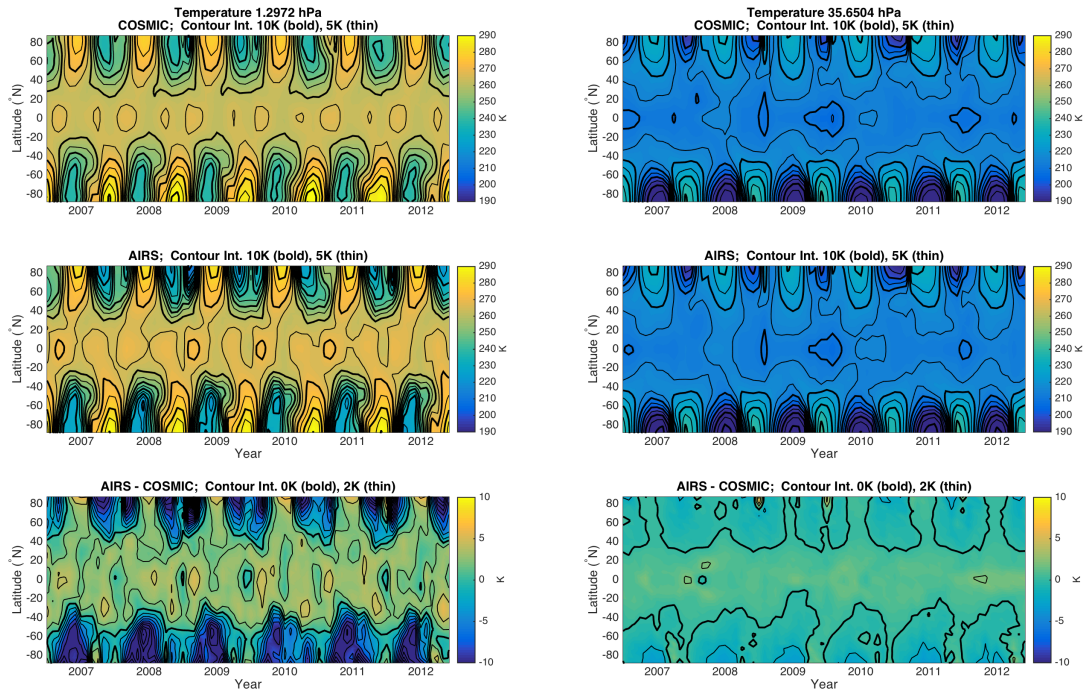


Fig 5. Monthly,  $5^\circ$  zonal number of samples for the  $-72.5^\circ\text{N}$  centered latitude zone for COSMIC (top, contoured by 500 counts) and AIRS (bottom, contoured by 5E5 counts).

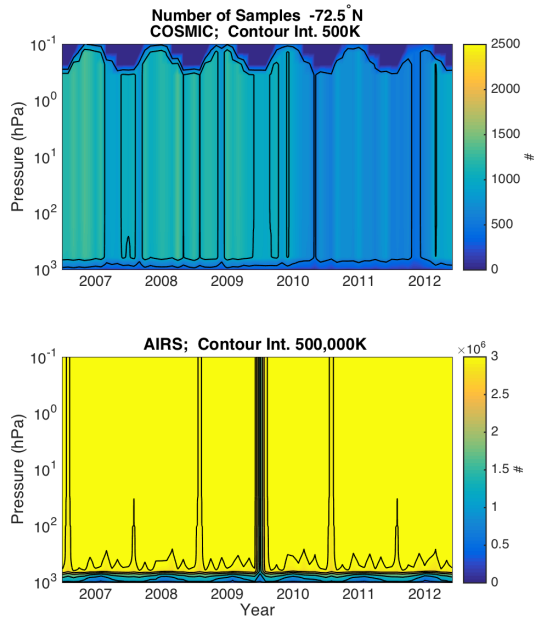


Fig 6. Monthly,  $5^\circ$  zonal standard deviation for the  $-72.5^\circ\text{N}$  (left) and  $2.5^\circ\text{N}$  (right) centered latitude zone for COSMIC (top) and AIRS (bottom) contoured by 10K (bold) and 5K (thin).

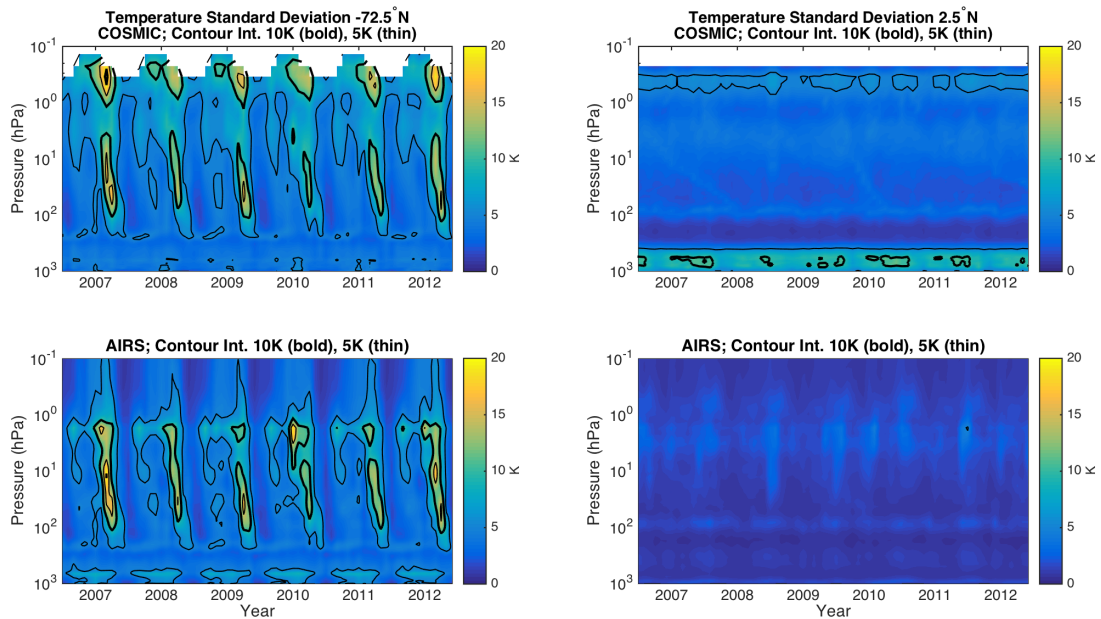


Fig 7. Monthly,  $5^\circ$  zonal  $72.5^\circ\text{N}$  (left) and  $-72.5^\circ\text{N}$  (right) COSMIC mean temperature (top, contoured every 20K), AIRS mean temperature (middle, contoured every 20K), and mean AIRS minus mean COSMIC difference (bottom, contoured bold at 0K and thin every 5K).

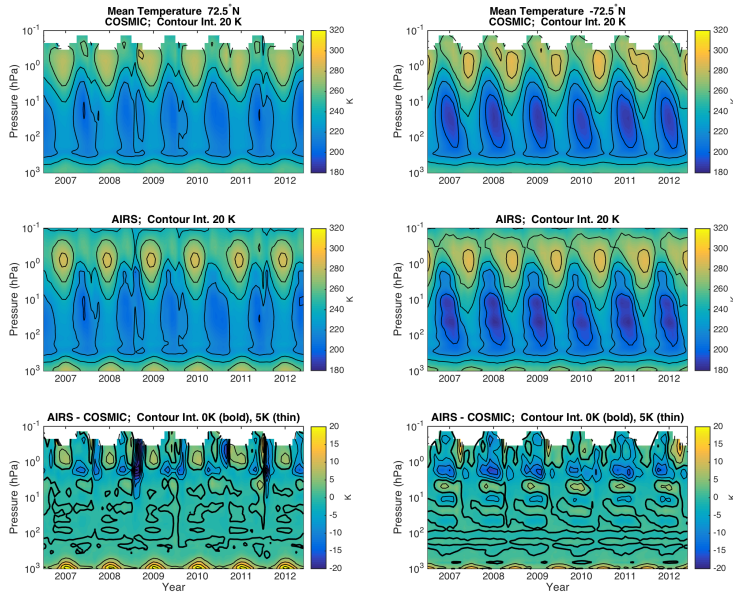


Fig 8. Monthly,  $5^\circ$  zonal  $47.5^\circ\text{N}$  (left column),  $2.5^\circ\text{N}$  (middle column)  $-47.5^\circ\text{N}$  (right column) COSMIC mean temperature (top row, contoured every 20K), AIRS mean temperature (middle row, contoured every 20K), and mean AIRS minus mean COSMIC difference (bottom row, contoured bold at 0K and thin every 5K).

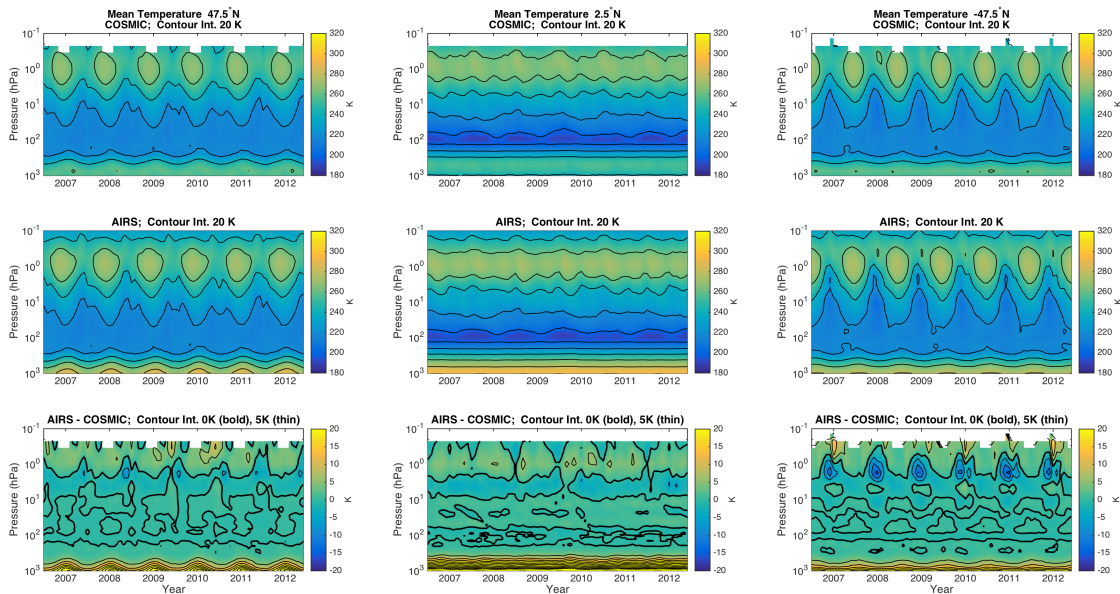


Fig 9. Five degree zonal, seasonal temperature climatology over 2007-2012 for DJF (left) and JJA (right) for COSMIC (top, contoured bold every 20K and thin every 10K), AIRS (middle, contoured bold every 20K and thin every 10K), and the AIRS minus COSMIC climatology (bottom, contoured bold at 0K and thin every 2K).

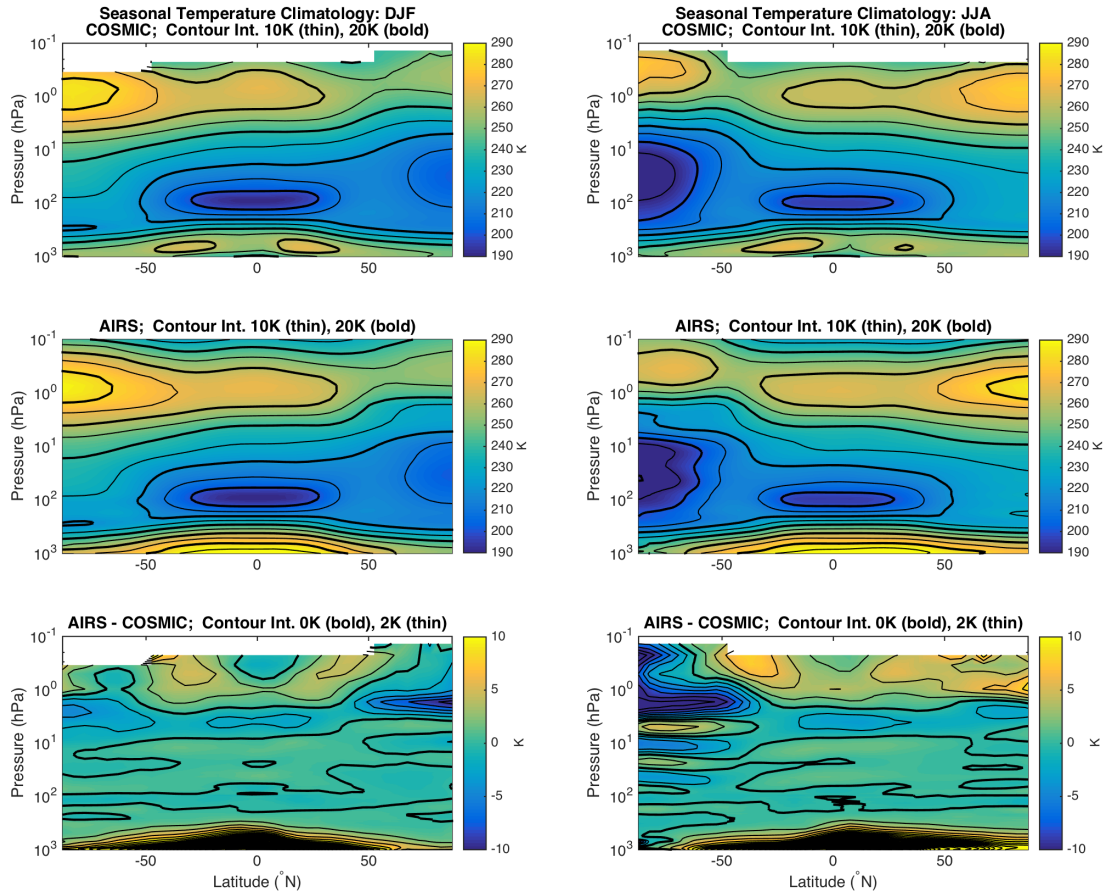


Fig 10. Histogram and normal distribution for mean monthly,  $5^\circ$  zonal mean AIRS minus mean COSMIC temperatures at  $\sim 1$ hPa (left) and  $\sim 35$ hPa (right) for the global (top) and  $\pm 20^\circ\text{N}$  tropical region (bottom), with the mean  $\mu$ , standard deviation  $\sigma$ , and uncertainty of the mean listed in the title. See Figure 4 for corresponding maps of differences.

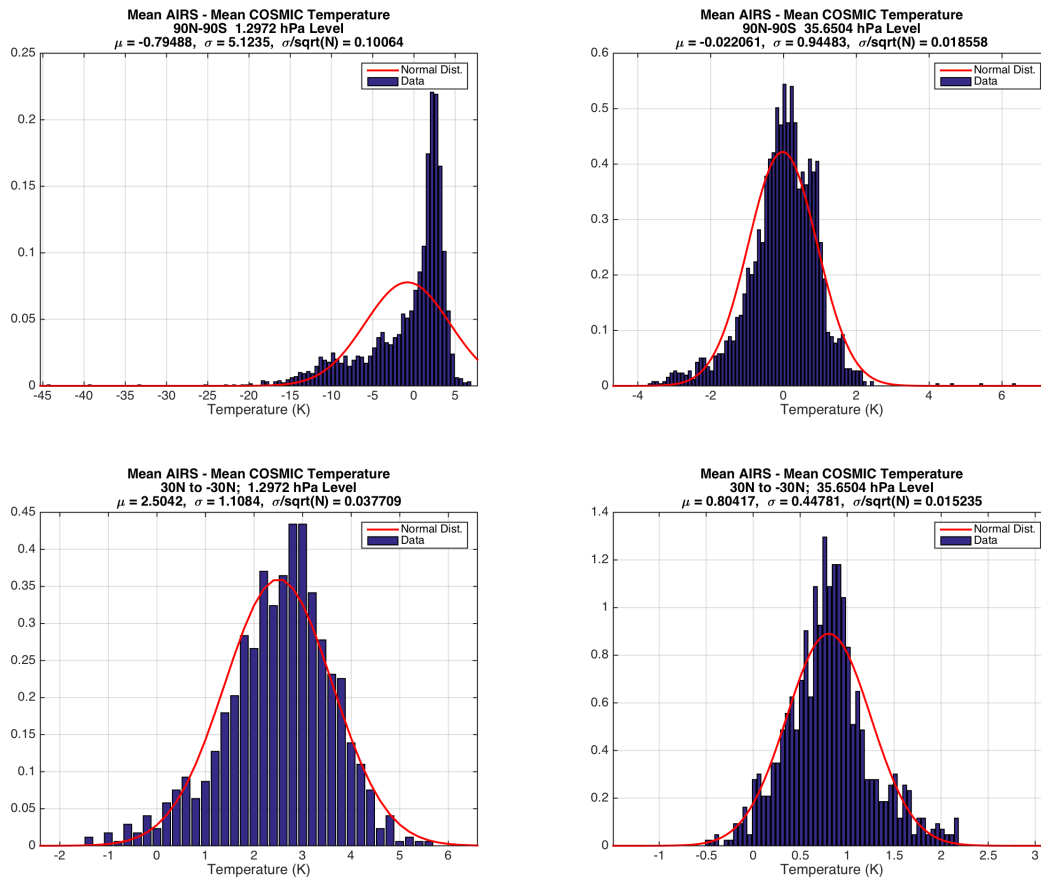


Fig 11. The 19 October 2007 locations of AIRS granule bounding boxes matched to COSMIC profiles within 1 hour shown as black squares, tangent points of COSMIC profiles matched to AIRS granules within 1 hour shown as red stars, and unmatched COSMIC profiles marked by blue dots.

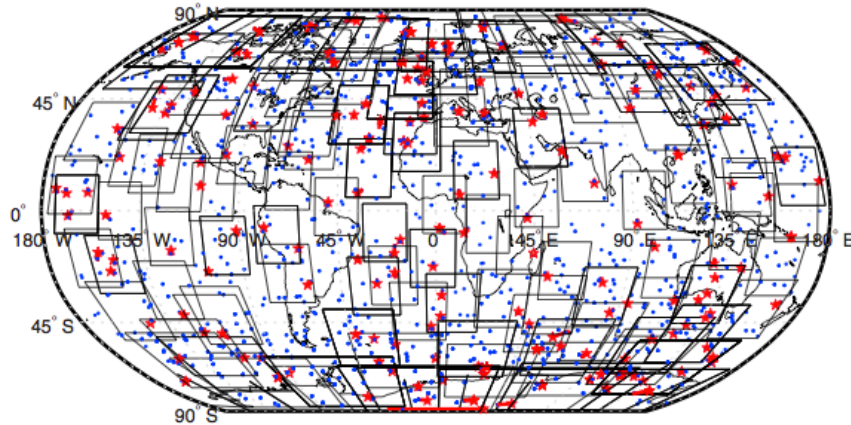


Fig 12. Example matchup case AIRS Level 1B  $667.782 \text{ cm}^{-1}$  matchup brightness temperatures (dots colored by Kelvin) and location of COSMIC profile (black dots).

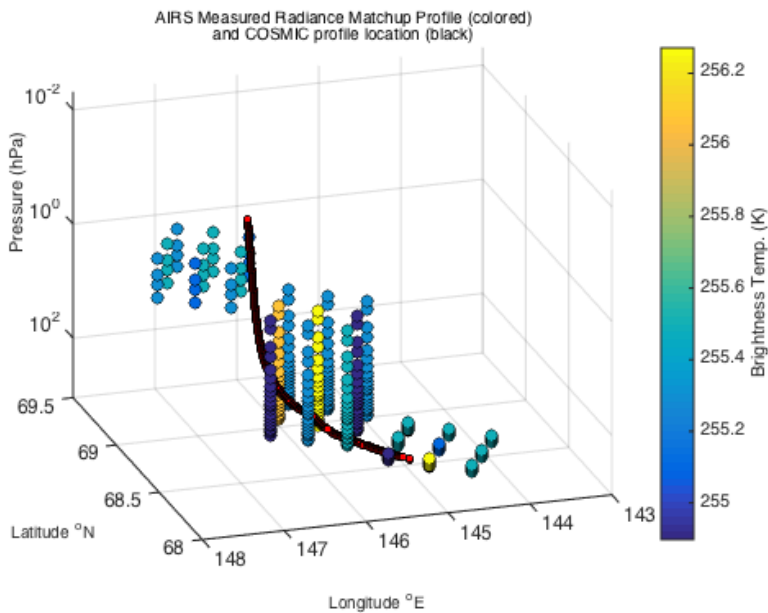


Fig 13. AIRS temperature Jacobian for the AFGL Mid-Latitude Winter temperature profile for the set of channels analyzed in this study. Dots indicate channels whose weighting function maxima occur at  $\sim 1$ hPa and  $\sim 35$ hPa.

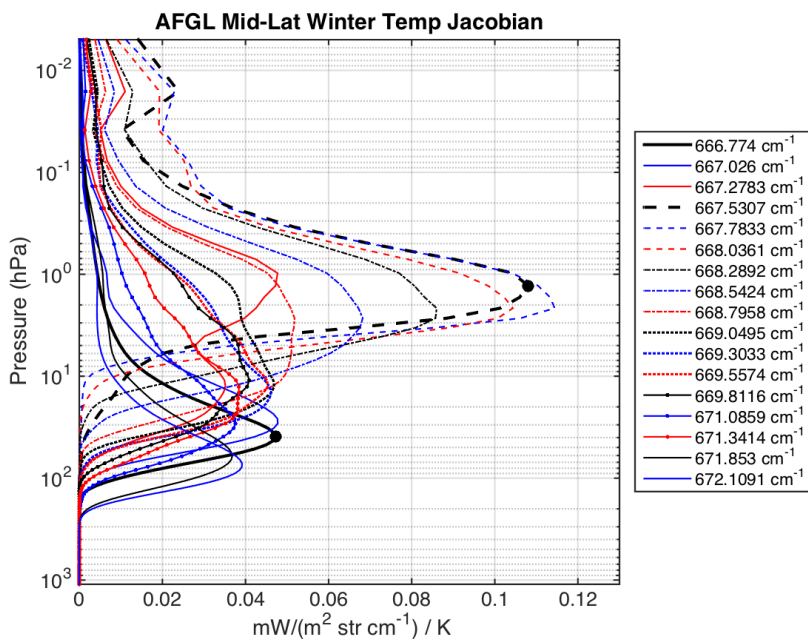


Fig 14. Averaging kernel calculated from the above weighting function and corresponding set of channels.

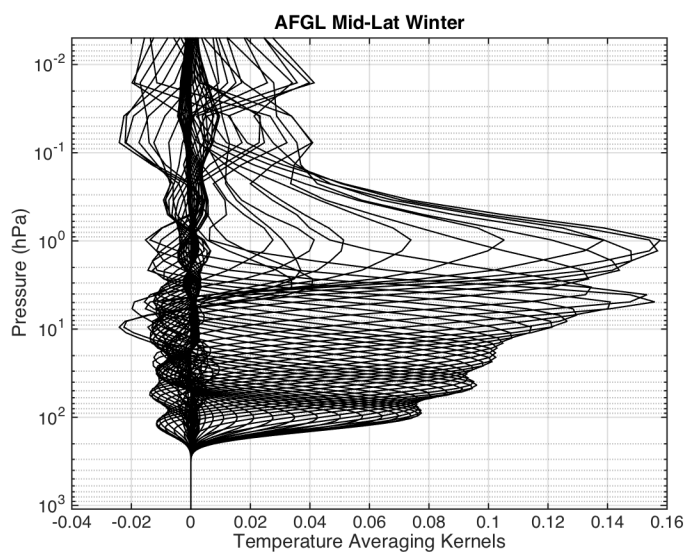


Fig 15. (Top) November 4<sup>th</sup> 2012 ~19UTC Madison UWSSEC radiosonde (green), COSMIC (red), CrIMSS (cyan), and AIRS (black) profile matchup case map, with surface points of sonde and COSMIC profile shown as stars and sounder profiles included in raypath-average profiles shown as stars. (Bottom) November 4<sup>th</sup> 2012 Madison matchup case temperature profiles overlaid with the CDAAC ERA-Interim.

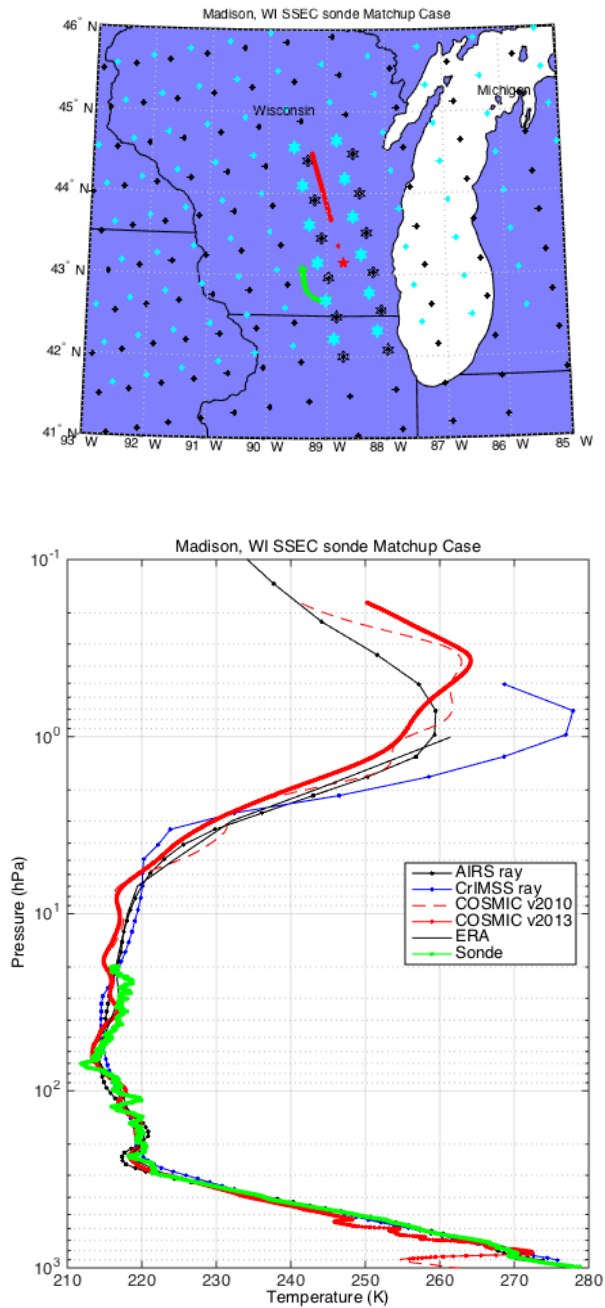


Fig 16. December 24<sup>th</sup> 2010 ~01UTC Tropical West Pacific Nauru Island ARMSite matchup COSMIC (red), AIRS (blue), and ARMsonde (black) overlaid temperatures (left) and a zoomed view of overlaid temperatures at the tropopause (right).

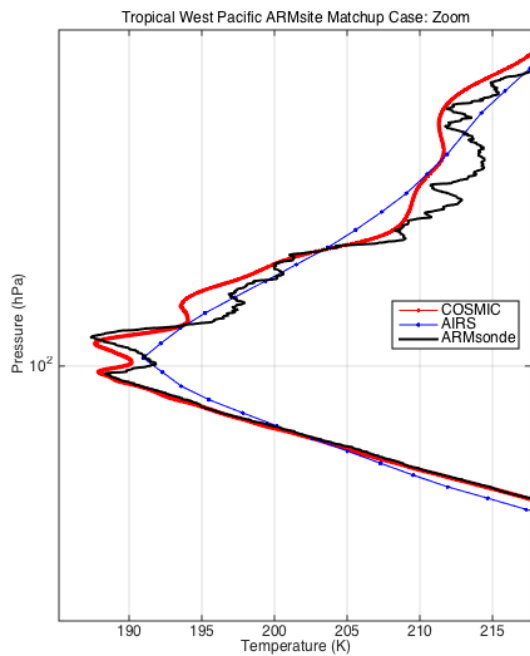
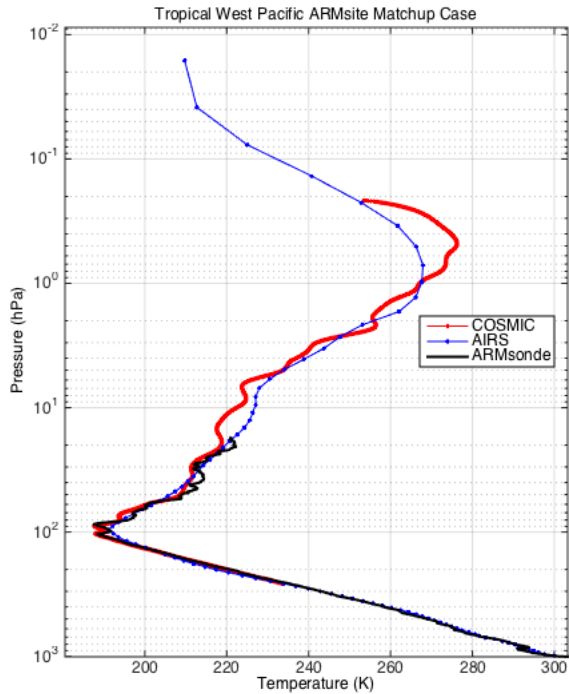


Fig 17. Control and perturbation CO<sub>2</sub> profiles (left) and resulting percent differences of the calculated perturbation minus control temperature Jacobians (right).

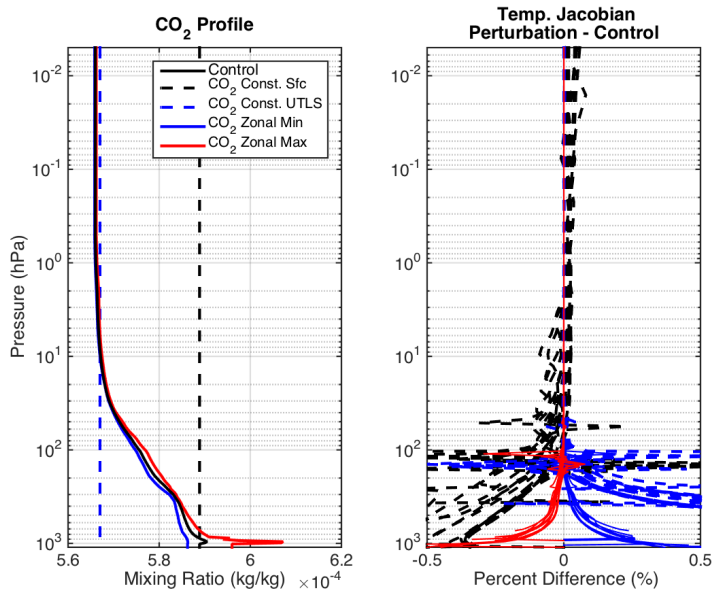


Fig 18. Carbon dioxide study control and perturbation computed BTs (top) and perturbation minus control BT differences, with circles marking locations of channels (bottom).

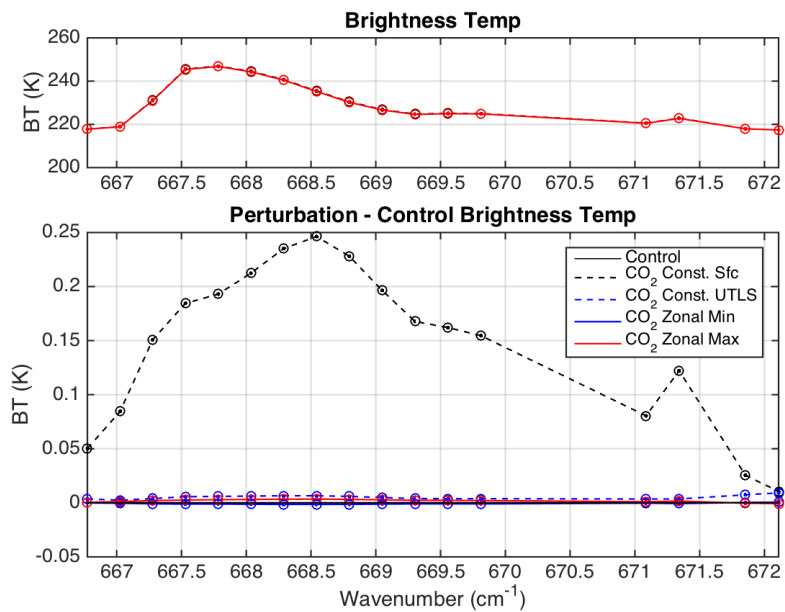


Fig 19. Control and perturbation temperatures (right), perturbation minus control temperature differences (middle), and resulting percent differences of the calculated perturbation minus control temperature Jacobians (left).

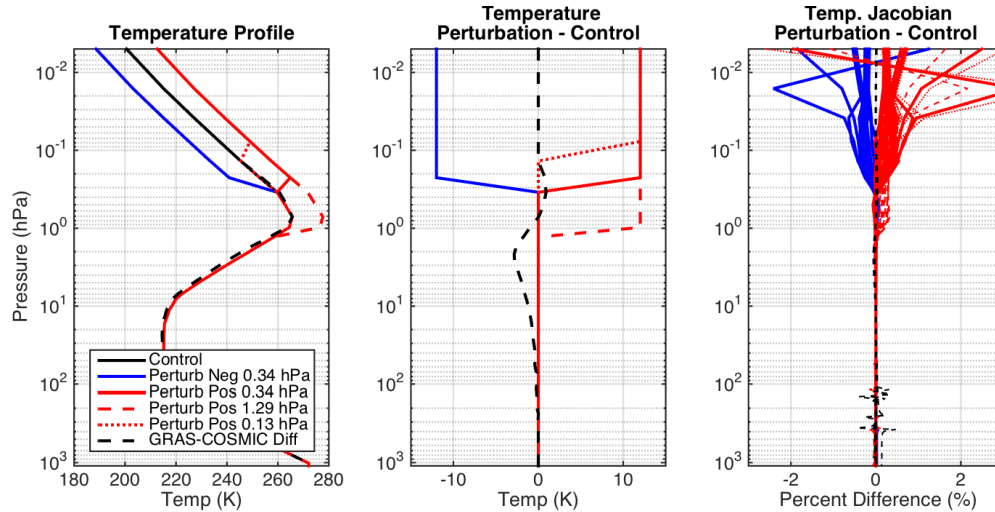


Fig 20. Temperature study control and perturbation computed BTs (top) and perturbation minus control BT differences with filled circles indicating locations of channels analyzed in subsequent analyses (bottom).

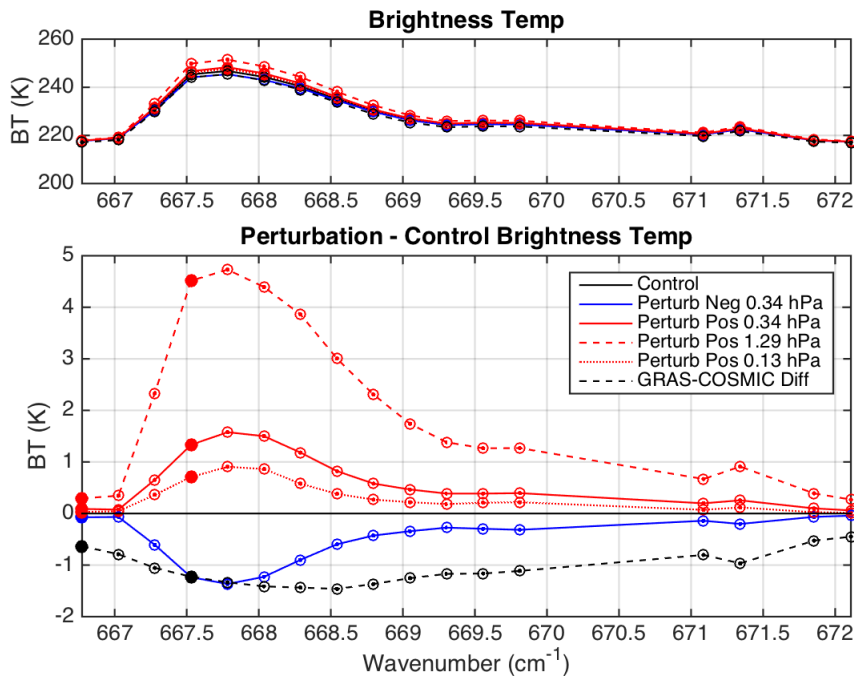


Fig 21. Matchup set monthly, 5° zonal ~1hPa (left) and ~35hPa (right) COSMIC mean temperature (top, contoured bold every 10K and thin every 5K), AIRS mean temperature (middle, contoured bold every 10K and thin every 5K), and AIRS minus COSMIC mean differences (bottom, contoured bold at 0K and thin every 2K). (X-axis year tick marks are centered on July 1<sup>st</sup>.)

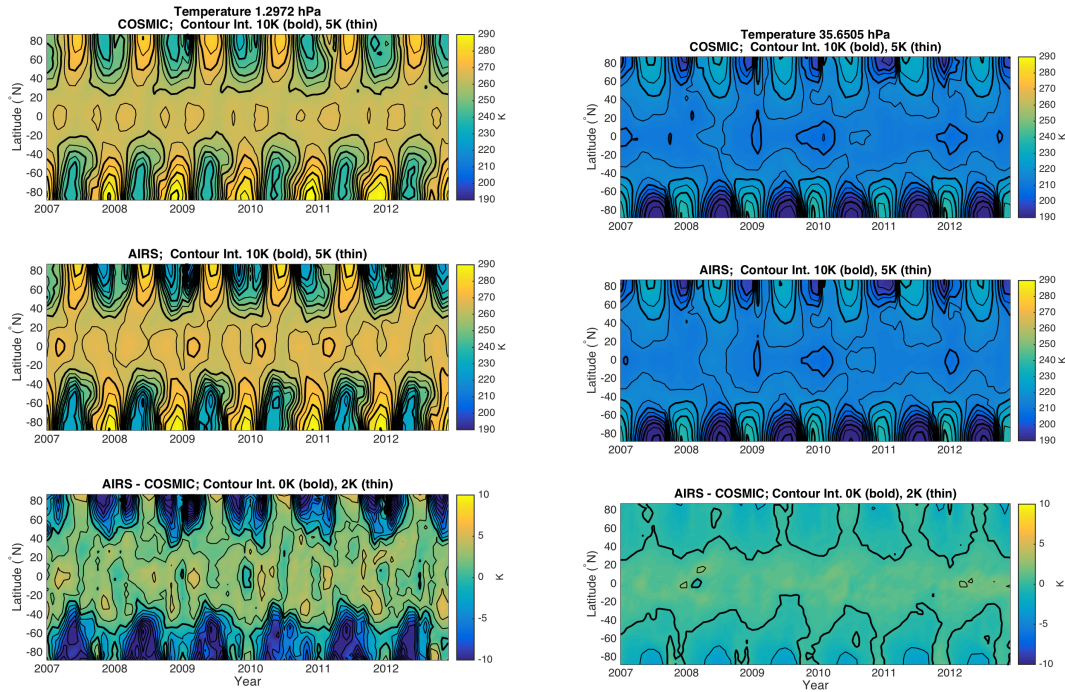


Fig 22. Histogram and normal distribution for the matchup set mean monthly, 5° zonal AIRS minus COSMIC mean temperatures at ~1hPa (top) and ~35hPa (bottom) for all latitude zones (top) and latitude zones within 20°N to -20°N (bottom), with the mean  $\mu$ , standard deviation  $\sigma$ , and uncertainty of the mean listed in the title. See Fig 21 for corresponding maps of differences.

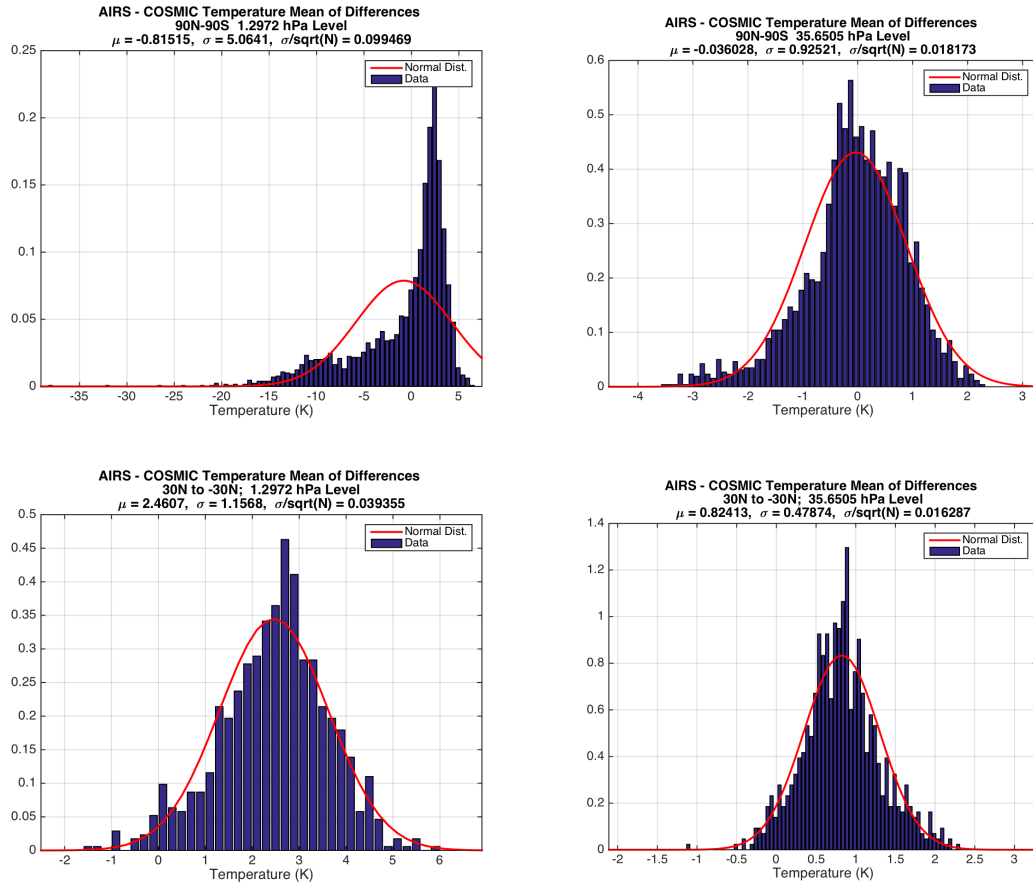


Fig 23. AIRS minus COSMIC 30°N to -30°N (left) and -90°N to -60°N (right) zonal temperature time series at ~1hPa (top) and ~35hPa (bottom) resampled 12 times per day (blue), daily filtered (green), 30-day filtered (red), and best fit one degree polynomial (dashed) with uncertainty (dotted). (X-axis year tick marks are centered on July 1<sup>st</sup>.)

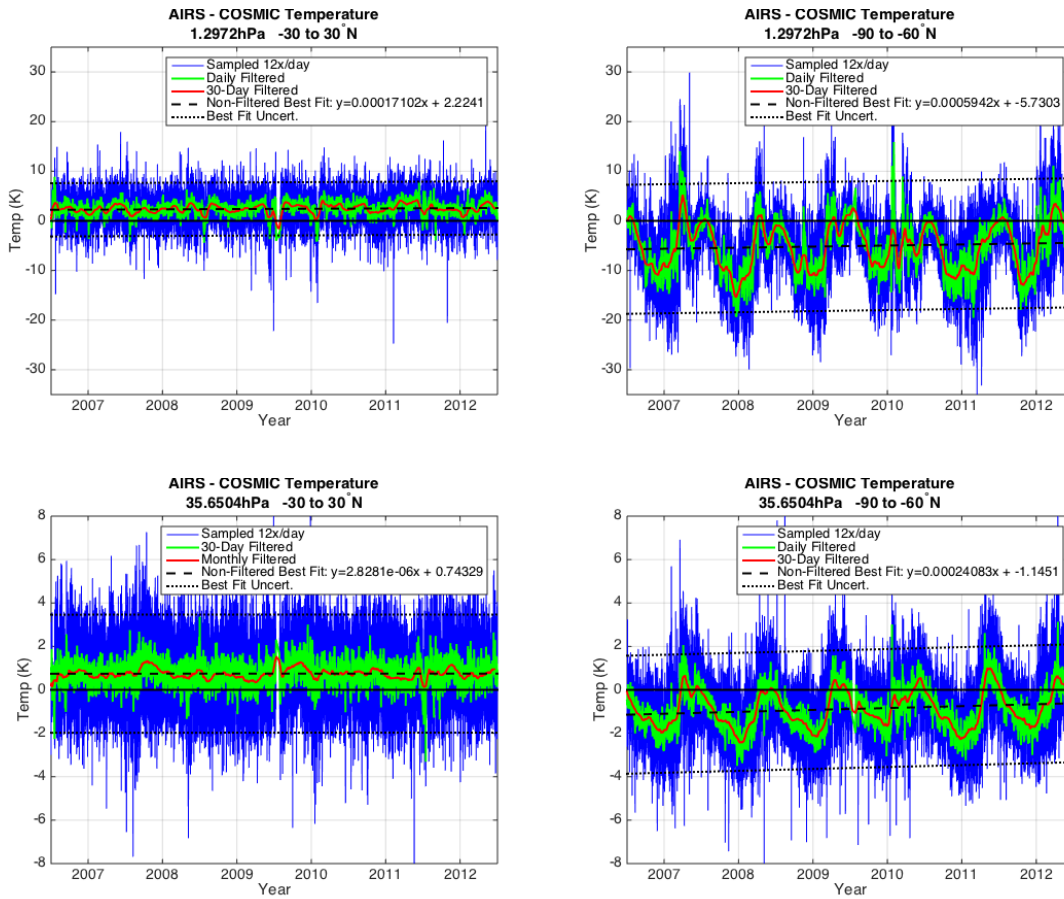


Fig 24. AIRS minus COSMIC 30-day filtered vertically smoothed (bold) and non-smoothed (thin) temperature time series at  $\sim 1\text{hPa}$  (top) and  $\sim 35\text{hPa}$  (bottom) for  $90^\circ\text{N}$  to  $60^\circ\text{N}$  (blue),  $30^\circ\text{N}$  to  $-30^\circ\text{N}$  (red), and  $-60^\circ\text{N}$  to  $-90^\circ\text{N}$  (black). (X-axis year tick marks are centered on July 1<sup>st</sup>.)

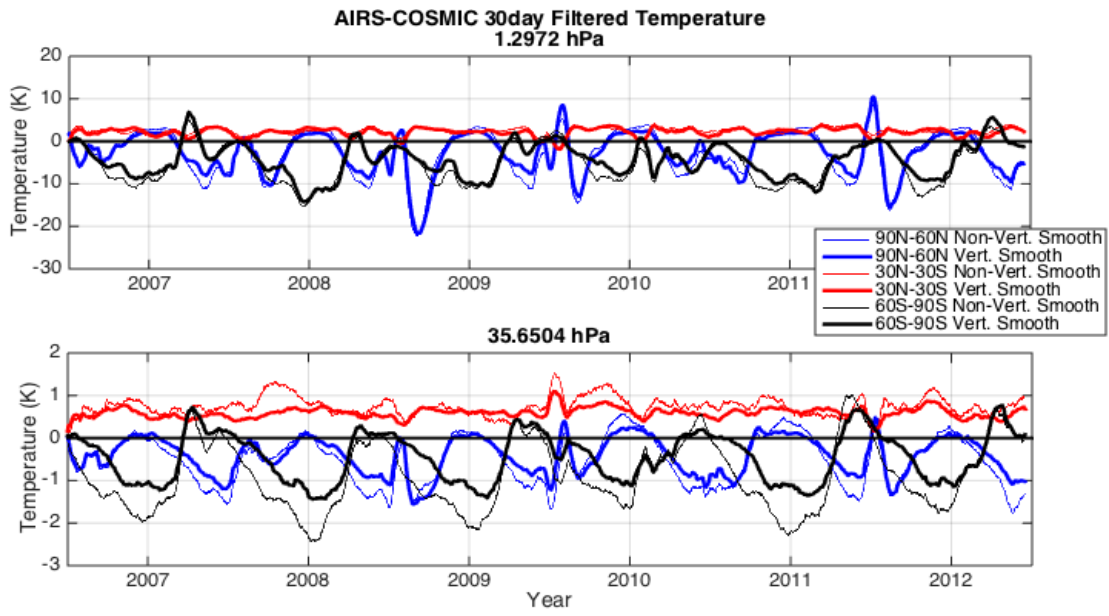


Fig 25. 30 day filtered  $\sim 1\text{hPa}$  level time series of COSMIC-minus-AIRS vertically smoothed temperature (black),  $667.5\text{cm}^{-1}$  channel AIRS calculated-minus-AIRS measured BT (red), and  $667.5\text{cm}^{-1}$  channel COSMIC calculated-minus-AIRS measured BT (blue) for the global and all 5 latitude zones. Adjusted BT differences (see text) are overlaid as dotted lines. (X-axis year tick marks are centered on July 1<sup>st</sup>.)

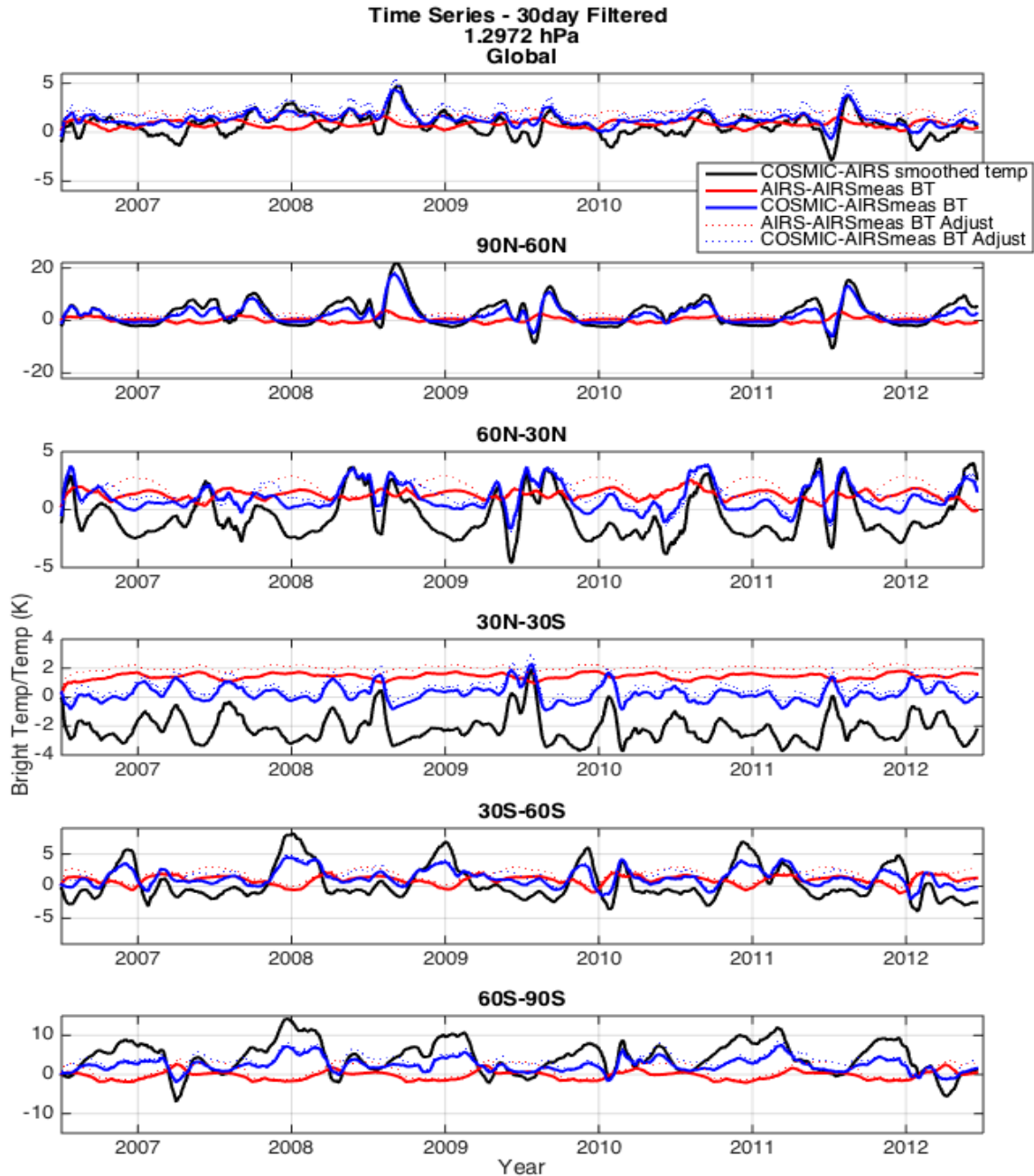


Fig 26. Same as above Fig 25 except for  $\sim 35$  hPa level and  $666.7\text{cm}^{-1}$  channel.

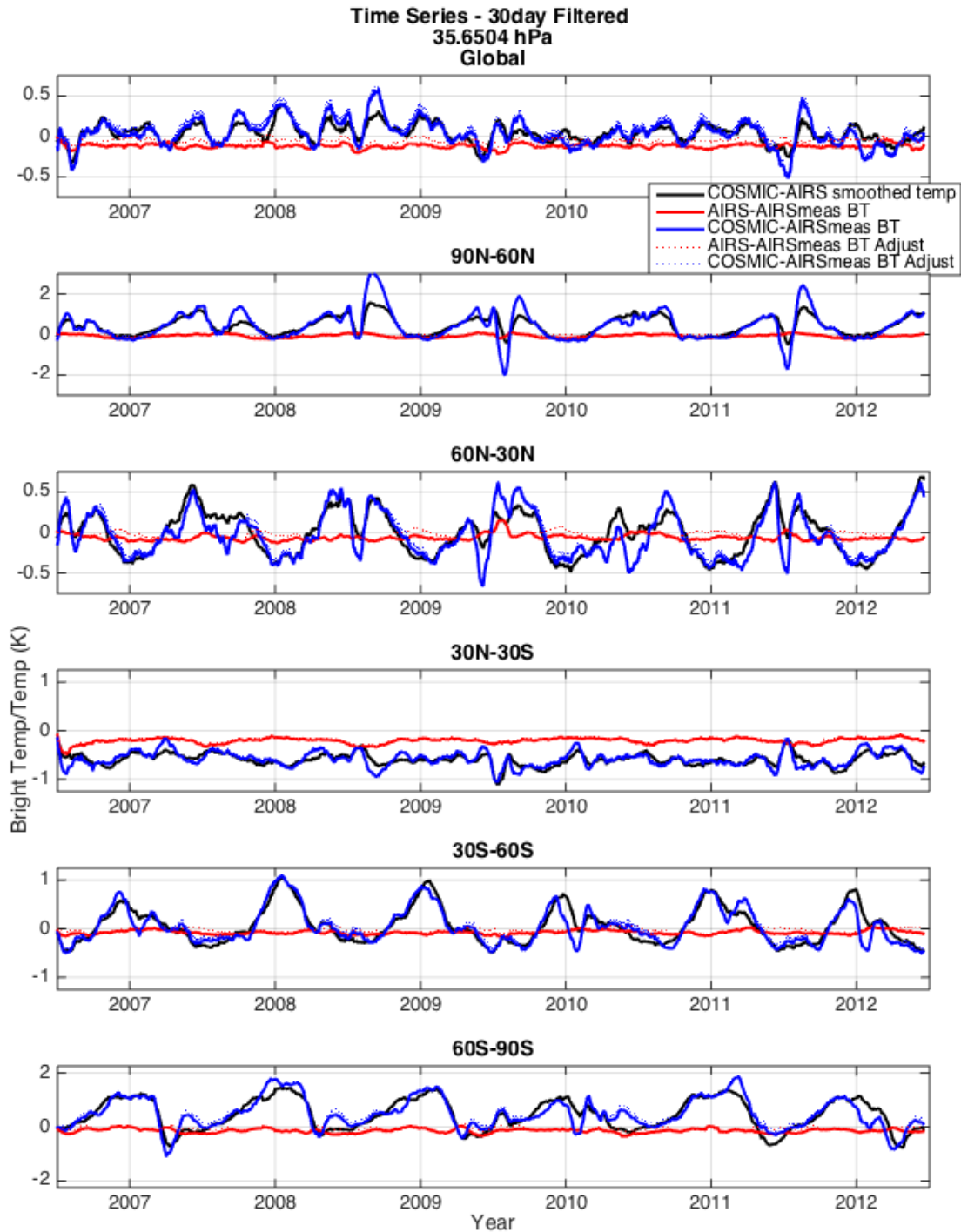


Fig 27. DJF brightness temperature (left panels) and temperature (right panels) differences for 6 different latitude zones. COSMIC calculated minus AIRS measured (black) and AIRS calculated minus AIRS measured (blue) BTs are shown at the pressure levels of the channels weighting function maxima and are overlaid with horizontal error bars representing the uncertainty of the mean and vertical error bars representing the full width at half max of the WF. Vertically smoothed (black solid) and non-smoothed (red solid) AIRS minus COSMIC temperatures are shown with their uncertainty of the means bounding them (dashed lines).

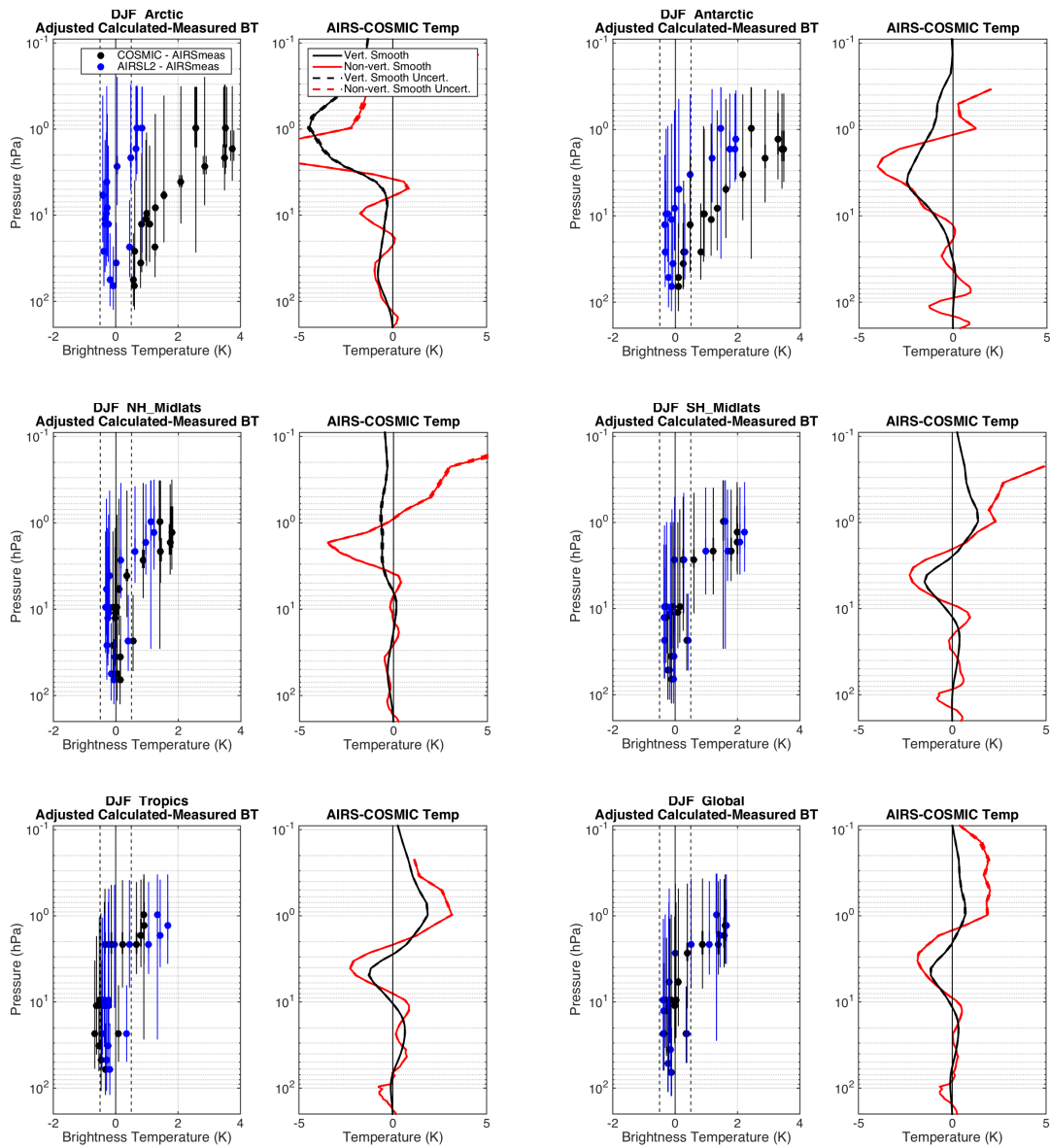


Fig. 28 Same as Figure 27 expect for JJA.

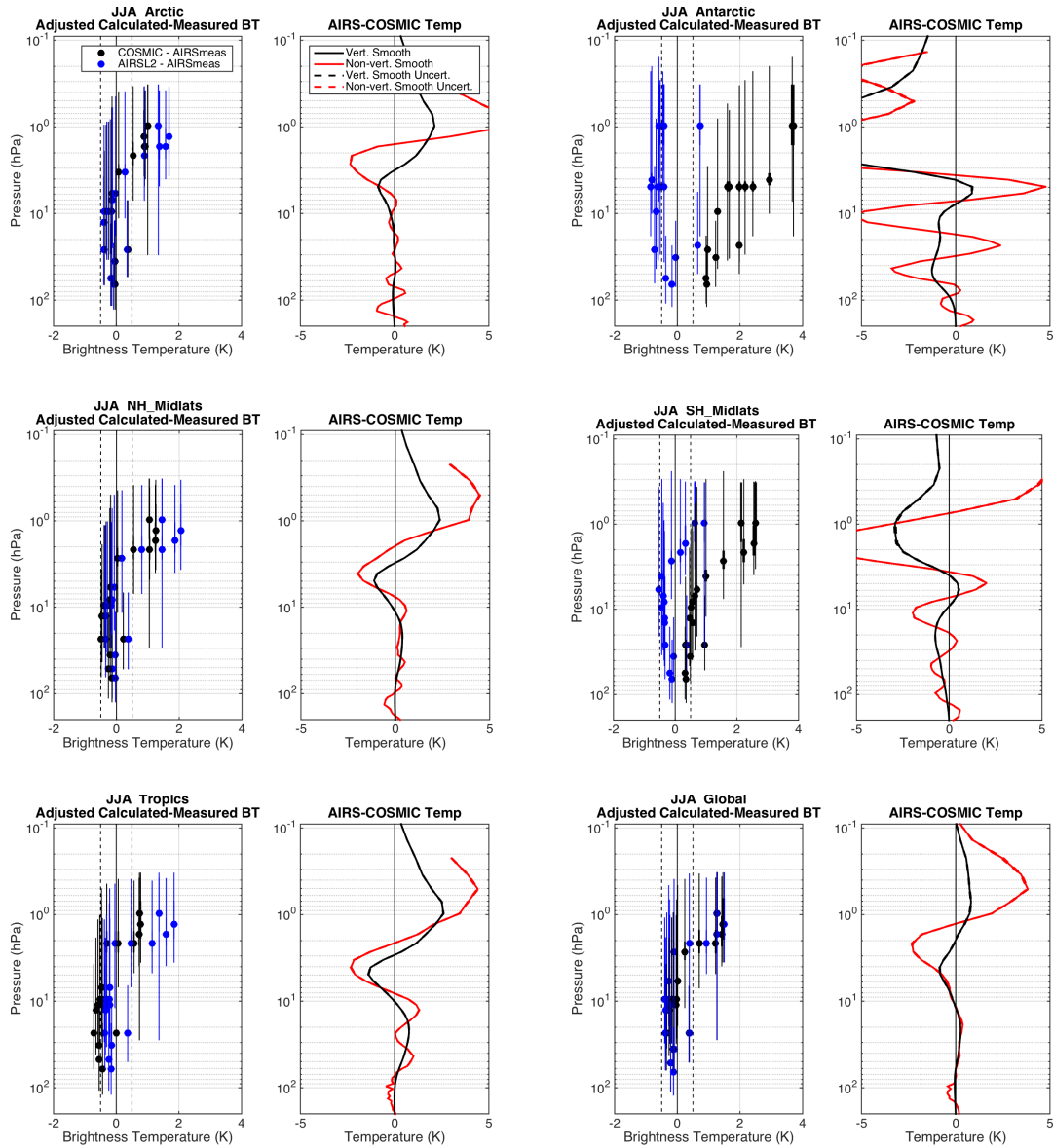


Fig 29. Monthly,  $5^\circ$  zonal  $666.7\text{cm}^{-1}$  channel (representing  $\sim 35\text{hPa}$ ) COSMIC calculated minus AIRS measured BTs (top, contoured bold every 1K and thin every 0.5K) and AIRS calculated minus AIRS measured BTs (bottom, contoured bold every 0.5K and thin every 0.1K). Note different color scale limits. (X-axis year tick marks are centered on July 1<sup>st</sup>.)

